Surface-Shaving Proteomics of *Mycobacterium marinum* Identifies Biofilm Subtype-Specific Changes Affecting Virulence, Tolerance and Persistence

Kirsi Savijoki[a]*, Henna Myllymäki[b]*,, Hanna Luukinen[b], Lauri Paulamäki[b], Leena-Maija Vanha-aho[b], Aleksandra Svorjova[b], Ilkka Miettinen[a], Adyary Fallarero[a,***], Teemu O. Ihalainen[b], Jari Yli-Kauhaluoma[d], Tuula A. Nyman[d], Mataleena Parikka[b#]**

a) Drug Research Program, Division of Pharmaceutical Biosciences, Faculty of Pharmacy, FI-00014, University of Helsinki, Finland
b) Faculty of Medicine and Health Technology, FI-33014 Tampere University, Finland
c) Drug Research Program, Division of Pharmaceutical Chemistry and Technology, Faculty of Pharmacy, University of Helsinki, FI-00014, Finland
d) Institute of Clinical Medicine, Department of Immunology, Faculty of Medicine, Rikshospitalet, University of Oslo and Oslo University Hospital, Norway

[#] **Correspondence to:** Mataleena Parikka
Email: mataleena.parikka@tuni.fi
Tel: +358 40 735 5052

***** These authors contributed equally to this work

****** Current address: UoE Centre for Inflammation Research, Queen's Medical Research Institute, University of Edinburgh, United Kingdom

******* Current address: Thermo Fischer Scientific, Ratastie 2, 01620 Vantaa, Finland

Running title: *Mycobacterium marinum* cell-surface proteome profiling

ABSTRACT (250 words)

The complex cell wall and biofilm matrix (ECM) act as key barriers to antibiotics in mycobacteria. Here, the ECM-proteins of *Mycobacterium marinum* ATCC927, a non-tuberculous mycobacterial model, was monitored over three months by label-free proteomics and compared with cell-surface proteins on planktonic cells to uncover pathways leading to virulence, tolerance, and persistence. We show that ATCC927 forms pellicle-type (PBFs) and submerged-type (SBFs) biofilms after two weeks and two days of growth, respectively, and that the increased CelA1 synthesis in this strain prevents biofilm formation and leads to reduced rifampicin tolerance. The proteomic data suggests that specific changes in mycolic acid synthesis (cord factor), Esx1-secretion, and cell-wall adhesins explain the appearance of PBFs as ribbon-like cords and SBFs as lichen-like structures. A subpopulation of cells resisting the 64 × MIC rifampicin (persisters) were detected in both biofilm subtypes, and already in one-week-old SBFs. The key forces boosting their development could include subtype-dependent changes in asymmetric cell division, cell wall biogenesis, tricarboxylic acid/glyoxylate cycle activities, and energy/redox/iron metabolisms. The effect of varying ambient oxygen tensions on each cell type and non-classical protein secretion are likely factors explaining majority of the subtype-specific changes. The proteomic findings also imply that Esx1-type protein secretion is more efficient in PL and PBF cells, while SBF may prefer both the Esx5- and non-classical pathways to control virulence and prolonged viability/persistence. In conclusion, this study reports a first proteomic insight into aging mycobacterial biofilm-ECMs and indicates biofilm subtype-dependent mechanisms conferring increased adaptive potential and virulence on non-tuberculous mycobacteria.

IMPORTANCE (88 words)

Mycobacteria are naturally resilient and mycobacterial infections are notoriously difficult to treat with antibiotics, with biofilm formation being the main factor complicating the successful treatment of TB. The present study shows that non-tuberculous *Mycobacterium marinum* ATCC927 forms submerged- and pellicle-type biofilms with lichen- and ribbon-like structures, respectively, as well as persister cells under the same conditions. We show that both biofilm subtypes differ in terms of virulence-, tolerance- and persistence-conferring activities, highlighting the fact that both subtypes should be targeted to maximize the power of antimycobacterial treatment therapies.

INTRODUCTION (5735 words)

Tuberculosis (TB) remains a major global health issue, with approximately 10 million new cases and 1.4 million deaths in 2019 (1). The causative agent, *Mycobacterium tuberculosis* (Mtb), is carried by an estimated one quarter of the human population as a latent infection, which has a 5–10% lifetime risk of developing into TB disease. In addition, the emergence of drug-resistant Mtb strains continues to be a public health threat, with about half a million new cases in 2019. Even in the case of drug-sensitive Mtb strains, the first line antibiotic treatment requires the use of four antimicrobials over a course of at least six months (WHO 2020). Moreover, despite successful treatment, the recurrence of TB carries a substantial risk, especially among immunocompromised patients (2, 3). The heterogeneity of the standard treatment outcome is also evident in PET-CT images showing non-resolving and active lesions and the presence of Mtb mRNA in sputum samples. This suggests that a significant proportion of patients generate viable mycobacteria in their lungs even after clinically curative antibiotic treatment (4). In a rabbit TB model, it was further shown that the caseum of granulomas contains Mtb that are

highly tolerant to most anti-TB drugs (5). The complex mycobacterial cell wall, involving capsule and outer/inner membranes connected by a dense mycolyl-arabinogalactan-peptidoglycan with high lipid levels, is the main barrier that protects the bacterial cells against drugs (6). While the mechanisms leading to drug tolerance in TB have remained poorly understood, biofilm formation was recently indicated as one of the strategies to increase viability, tolerance and persistence (7-10).

Biofilm formation is defined as adherent growth within self-produced extracellular matrix/ECM consisting of proteins, polysaccharides, and DNA/RNA, and it is the strategy bacteria use to escape the effects of antibiotics and host defense systems (11-13). Mycobacteria use phenotypically distinct biofilm subtypes for growth, which genetically and physiologically differ from the planktonic-type growth. These include (i) floating/pellicle-type biofilms (PBFs) at the air-liquid interface having an ECM rich in free mycolic acids (MAs) and with a frequent cord/ribbon-like appearance, while (ii) submerged-type biofilms (SBFs) show adherent growth on a solid substratum (11, 14-16). The capsule layer plays a vital role in triggering biofilm growth in mycobacteria, as cells cultured in the presence of Tween-80 (non-ionic surfactant) has been shown to detach the capsule layer and prevent the biofilm formation (17). Thus, this labile layer forming the first molecular interaction with the host/environment is likely to involve key factors contributing to persistence/adaptation and search of anti-TB targets. Although several studies on mycobacteria have pinpointed cellular pathways and proteins that affect the capsule/cell wall and the biofilm formation (9, 14, 17-25), systematic investigation of the factors that directly interact with the surrounding environment is necessary to be able to maximize the power of antimycobacterial treatment therapies.

Mycobacterium marinum (Mmr) has proven to be an excellent alternative model pathogen for slow-growing Mtb, as it allows for the investigation of TB-like chronic and latent

infections in its natural host, the zebrafish (26-29). Cultured mycobacterial biofilms have been used to understand resilient bacterial phenotypes emerging in mycobacterial infections. However, the distinct phenotypic profiles associated with PBFs and SBFs, including marker proteins discriminating the two biofilm subtypes have remained poorly understood. To shed light on the specific attributes linking these biologically different biofilm subtypes to their phenotypes, we first cultured Mmr strain ATCC927 to create in vitro biofilms. These biofilms were then imaged using widefield deconvolution microscopy (WDeM) to investigate temporal effects on the biofilm architectures. Label-free quantitative (LFQ) proteomics was next used to uncover the ECM-proteome dynamics in maturing Mmr biofilms and to identify the cell surface proteins (proteome) on Mmr grown on Tween-80, a detergent known to prevent cells from clumping and forming a biofilm (17). The key proteome findings were validated by gene overexpression studies to indicate cellulose-dependent biofilm formation as well as biofilm killing assays to confirm the formation of persister cells in both biofilm subtypes. To the best of our knowledge, this is the first study monitoring mycobacterial ECM-proteomes over three months' time as well as protein and morphological phenotypic markers for distinguishing defined biofilm subtypes.

RESULTS

SBFs and PBFs show distinct morphological characteristics

The kinetics of development and maturation as well as the morphology of mycobacterial PBFs and SBFs has been reported to differ substantially (8). Here, we first show that that Mmr forms PBFs at the air-liquid interphase and SBFs attached onto the bottom of the culture well under the same physiological in vitro conditions after two weeks of growth **(Fig. 1SA)**. The SBF subtype develops earlier (visible already after two days of culture) than the PBF, which was not clearly distinguishable before two weeks of growth. Next, we

129 investigated the three-dimensional morphology of Mmr biofilms in more detail by culturing
130 Mmr cells, carrying the pTEC27 plasmid with the tdTomato fluorescent marker gene (29),
131 for two and three weeks to produce PBFs and SBFs, and analyzing the biofilms by
132 widefield deconvolution microscopy (WDeM). **Figure 1** shows that Mmr forms organized,
133 three-dimensional structures with distinctive, subtype-specific morphological features. For
134 the SBF, the structures displayed a lichen- or moss-like appearance, having tens of
135 microns high feature structures rising from the biofilm base after two weeks **(Fig. 1B)**. In
136 comparison, the morphology of the PBF subtype was very different by the first time point,
137 showing flat, ribbon-like structures without any protruding structures **(Fig. 1C)**. Defined,
138 extensive structures in all dimensions, although less dense compared to those detected at
139 the two-week-time point, were found for both biofilm subtypes also after three weeks of
140 growth.
141
142 **Submerged biofilms exhibit the greatest ECM-proteome diversity**
143 As the phenotypic profiles of PBFs and SBFs are clearly different, their ECM-proteomes
144 were next quantitatively monitored and compared during the development and maturation
145 stages. To this end, the PBF and SBF cells at the points in **Figure 2A** were subjected to
146 trypsin/Lys-C digestion as well as LC-MS/MS-based protein identification and LFQ (all
147 data available via PRIDE with identifier PXD02010). Logarithmic state planktonic cells
148 (PL_log), representing single-cell cultures, were obtained by growing the Mmr strain in the
149 presence of Tween-80. The quality of each data set was high: 84.7% or all proteins were
150 identified with at least three or more matching peptides, with an average sequence
151 coverage of approximately 31% and only 11% of proteins were categorized as single-
152 peptide-hits**.** In addition, a broad overlap in protein identifications was detected within the
153 four biological replica samples; 41-89 % of the proteins were shared by each replicate,

with the two-week PBF and the three-week SBF showing the highest variation between replicates **(Fig. S1B)**. **Table S1** lists the proteins detected in at least two out of four replica samples. An outlier replicate associated with one of the SBF identification replica sets at the three-week-timepoint was excluded from subsequent data analyses. The number of detected proteins was 1132, 1957, and 2133 for the PL, PBF and SBF cells, respectively.

Cytoplasmic protein export/release is most efficient in submerged biofilms

Figure S2A shows the distribution of all identified proteins according to their predicted secretion motif (Sec/SPII, TatP/SPI, LIPO/SPII, type VII secretion/T7SS, SecretomeP) and the number of transmembrane spanning domains (TMDs). The most notable differences were detected for membrane proteins with six to ten TMDs as well as in the number of cytoplasmic proteins. Nearly two-fold more TDM proteins were detected in the PL than the biofilm cells. In contrast, two-fold more cytoplasmic proteins predicted to be exported out of the cells via a non-classical route (SecretomeP) were identified from the biofilm-ECMs (*n*, 300) in comparison to the PL cells (*n*, 150). For many of these proteins, a secondary function as a moonlighting protein (30) could be indicated **(Table S1)**. In addition, over 900, 1600 and 1800 cytoplasmic proteins identified on the PL, PBF, and SBF cells, respectively, contained no motifs for classical or non-classical secretion and were assigned here as “Others” **(Table S1).**

Most significant protein abundance changes specific to planktonic and biofilm cells

The Venn diagram in **Figure S2B** indicates the highest number of specifically identified proteins on the SBFs (*n*, 173) and the lowest on the PBFs (*n*, 16), while no unique identifications were detected for the PL cells. The uniquely detected proteins with the highest raw intensity values included a signal transduction associated serine/threonine-

179 protein kinase (PknL), a LGFP-repeat protein specific to SBFs, and a β-1,3-endoglucanase
180 and bacterioferritin BfrA specific to PBFs **(Table S2)**. The proteins detected with the
181 highest intensity values and only in the biofilm-ECMs included an error-prone polymerase
182 DinB, a preprotein sec-translocase subunit YajC, a cytochrome P-450 monoxygenase, a
183 PE family immunogen and a signal transduction-related adenylate cyclase involved in
184 cyclic di-AMP biosynthesis **(Table S2)**.
185 Next, the log2 transformed MaxLFQ data was subjected to pairwise comparisons to
186 indicate statistically significant protein abundance changes **(Table S3)**. **Figure 3** shows
187 the greatest growth mode- and time-dependent fold-changes related for the PL vs. biofilms
188 cells, PBF vs. SBF cells and each biofilm subtype at different time points. Comparison of
189 the PL and both biofilm cells at their first timepoints of growth (PBF_2w and SBF_2d)
190 indicated the most prominent changes for PPE-family proteins (e.g., PPE61) and enzymes
191 involved in cell envelope biogenesis/metabolism (MurE, CwlM, cutinase and CelA1).
192 Among these, the PPE61 immunogen was *ca.* 6000- and 1800-times more abundant on
193 the PL compared to the PBF_2w and SBF_2d, respectively. CelA1, a β-1,4-
194 cellobiohydrolase known to prevent biofilm growth in *M. smegmatis* and Mtb (11, 18, 19),
195 was detected with 50- and 130-fold higher abundances on the PL compared to the PBFs
196 at the one-week and the SBFs at the two-day timepoints, respectively **(Table S3)**.
197 Comparison of the PBF_2w and SBF_2d cells indicated Esx1-associated virulence factors
198 (i.e., EspF, EspA/EspE and ESAT-6) and PPE family immunogens as 30–130-fold more
199 abundant on the PBF than the SBF cells, meanwhile tricarboxylic acid (TCA)/glyoxylate
200 cycle-associated isocitrate lyase (ICL1) was over 200-fold more produced by the SBF than
201 the PBF cells. After 12 weeks, the proteins more abundant in the SBF compared to the
202 PBF included an LppP/LprE lipoprotein (*ca.* 16-fold), HemD involved in the synthesis of
203 vitamin B12 (*ca.*15-fold), FadD29 contributing to the synthesis of phenolic glycolipids (~13-

fold), β-lactamase able to hydrolase β-lactam antibiotics (*ca.* 9-times) and ICL1 catalyzing the glyoxylate shunt-mediated activities (*ca.* 8-fold). More abundant proteins on the PBF at this time-point were identified as a polysaccharide (N-acetylmuramic acid, MurNAc) deacetylase PdaC (*ca.*15-fold) and a translocase subunit, SecE (*ca.*11-fold).

In the PBF, an MPB64 immunogen, siderophore export accessory protein MmpS5, several Esx1-associated proteins (EspA/EspE, EspF) and adhesins (Ala-Pro-Ala rich protein APA and fibronectin binding protein FAP) displayed the most significant abundance decreases at the 12-week timepoint. In the SBFs, these proteins included a large-conductance mechanosensitive channel protein Msc, a membrane protein acting as the cells' safety valve to relieve osmotic pressure, arabinosyltransferases EmbA/EmbB, the Esx1 associated EspA/EspE and the MycP1 protease. Proteins with the greatest abundance changes after 12 weeks in the SBFs included mammalian entry proteins (MCEs) and an α-1,4-glucan:maltose-1-phosphate maltosyltransferase.

Decreased CelA1 synthesis is also required for biofilm formation in *M. marinum*

As our findings suggest that a lack of CelA could also promote the biofilm formation in Mmr, we tested this hypothesis by overexpressing the *celA1* gene in a Mmr strain equipped with pTEC27 with the tdTomato fluorescent marker (29). First, the *celA1* expression level in the transformed Mmr strain was confirmed by qPCR, indicating a *ca.* 150-times higher *celA1* transcription compared to the control strain carrying an empty pTECV27 **(Fig. 4A).** Then we analyzed the morphology of both the SBFs and PBFs after two weeks using the CelA1-strain with WDeM. As seen in **Figure 4B**, the CelA1-strain showed altered morphology compared to the Mmr with pTEC27 (WT control strain). After two weeks of growth the CelA1-strain SBF showed a less defined/loss of the lichen-like morphology and lower total thickness when compared to the SBF control with pTEC27.

Similarly, the CelA1 overproduction in Mmr resulted in disrupted and fuzzy ribbon-like cords associated with PBF-type biofilm growth, as the PBF cells with pTEC27 had well defined and tight ribbon like structures.

CelA1 expression was recently linked with biofilm formation, antibiotic tolerance, and virulence in Mtb (9). Therefore, Mmr cells in planktonic and biofilm forms with/without the CelA1 overexpression were also exposed to rifampicin to determine the minimum inhibitory (MIC) and minimum bactericidal concentration (MBC) for this bactericidal first-line TB drug. **Figure 4C** shows that, in both the planktonic and biofilm cultures, CelA1 overexpression decreases the MIC/MBC, with a clear impact on two-day-old and 4-day-old biofilms. These results indicate that CelA1 impedes biofilm formation and increases the susceptibility of the residing cells to rifampicin in Mmr.

Functional pathways specifically induced in planktonic and biofilm cells

The LFQ proteomic data was next subjected to a PCA analysis for comparing growth mode- and time-dependent protein abundance patterns on the PL cells and aging biofilms. The PCA in **Figure 5A** shows clear clustering for each data set except for replicates associated with two-week-old PBF-proteomes, which show greater variation. PC1, separating the samples according to the growth mode, explains 39% of the total variation, while 24% (PC2) of the variation can be explained by the age of the culture. The two-day-old SBF-proteomes form a clearly distinguishable cluster, while the PL-proteomes and proteomes associated with the PBFs between the two- and four-week time-points show close clustering. Although the SBF- and PBF-proteomes differ greatly within the first four weeks of growth, these biofilm subtypes seem to undergo similar proteome changes during the later stages of growth, as proteomes of both subtypes clustered more closely at the 12-week timepoint. Notably, PBFs during the first weeks (two to three weeks) of growth

shared a more similar ECM-proteome with the PL cells than the SBFs under the same conditions.

Next, a multi-sample test (ANOVA) was conducted on the normalized LFQ intensity data to investigate growth mode-dependent proteome differences at time points between two days and three months. A dendrogram/ heatmap in **Figure 5B** shows hierarchically clustered co-abundance data for 690 proteins having a statistically significant abundance change in at least one of the conditions tested **(Table S4)**. Six major clusters were clearly distinguished, among which cluster 1 (*n*, 375) and cluster 6 (*n*, 125) contained the greatest number of proteins, with higher abundances in one- to four-week-old SBFs (cluster 1) and two-day- to two-week-old SBFs (cluster 6), respectively. STRING (Search Tool for the Retrieval of Interacting Genes/Proteins) enrichment analyses performed on both clusters **(Table S5)** indicated the greatest changes for pathways coordinating cell envelope biogenesis/ metabolism, energy metabolism and protein secretion/export. **Figure 6A** shows a protein-protein interaction (PPI) network for cluster 1 proteins: **(i)** cytoplasmic proteins with a primary function in amino acid biosynthesis (*e.g.*, Gly, Asp, Tyr, Arg, His, Thr, Ser, Lys, Phe), purine/pyrimidine metabolism (*e.g.*, PyrG, PurD/L/H, GuaB) and stress response (HrcA, ClpC/X, DnaJ, HtpG, AhpC, SodC, RecA, Trx), **(ii)** proteins involved in cell-wall/outer layer and mycomembrane biogenesis/metabolism (*e.g.*, PknA/B, Weg31, CwsA, CwlM, PbpA1a, EmbA/B, KasA, DesA1/2, PpsA/B/D, PcaA, Fad enzymes), **(iii)** components of the respiratory electron transport chain (SDH, FMR, Qcr-complex) and ATP synthesis (F1F0 ATP synthase-complex), and **(vi)** proteins involved in iron storage/homeostasis (ferritin). The PPI network analysis on the cluster 6 proteins indicated the enrichment of metabolic activities related to translation (ribosomal proteins/r-proteins), stress response (GroEL/ES, GrpE, DnaK, TF, ClpB) and the TCA/glyoxylate cycle (*e.g.*, CitA, ICL1, FBA, GlcB) **(Fig. 6B)**.

Clusters 2, 4 and 5 (*n,* 144) share co-abundance patterns, which indicate increased protein abundances during the first weeks of growth in the PBFs when compared to the SBFs. These contain virulence-, invasion- and viability/persistence-related proteins, such as EsxA/B, ESX-EspB/G/M/P/N, Esx5-secretion associated protease MycP, cutinase (Cut), a lysophospholipase (YtpA), endopeptidase (Lon), heparin binding hemagglutinin (HbhA), fibronectin binding (Apa), catalase-peroxidase (KatG), and mammalian entry proteins (MCEs). Cytoplasmic proteins were also detected in these clusters (e.g., ICL2, ACN, ENO, GapDH, GPD, Tpi, PGK, MDH, ClpP1/2, CpsA/D, Trp, Cys, Met, an 18-kDa β-CA) but their composition differs clearly from those in clusters 1 and 6. In addition, cluster 2 contains virulence-associated ESAT-6-like proteins, TDM-cord factor synthesis associated Ag85A/C (mycolyltransferases), and an MPT64 immunogen with higher overall abundancies on the PL and PBF cells compared to the SBFs. The remaining cluster 3 (*n*, 47) differs from the other five by proteins with its overall higher abundancies on the PL cells and/or on four- to 12-week-old PBFs when compared to the SBFs at the same timepoints. One of these was identified as a potential trehalase (A0A2Z5YJK7_MYCMR), a glycoside hydrolase that catalyzes the conversion of trehalose to glucose, which had a high abundancy in four- and 12-week-old PBFs.

The protein identifications most relevant to biofilm growth and viability identifications are listed in **Table S6** according to their predicted functions. The major growth mode-dependent changes associate with the following five functional groups: **(i)** secretion mechanisms, virulence, and adherence; **(ii)** cell wall/membrane/lipid biogenesis and metabolism and biofilm formation; **(iii)** stress response; **(iv)** TCA/glyoxylate cycles and carbohydrate metabolism; and **(v)** maintaining redox balance and energy metabolism. An additional schematic model of the mycobacterial cell envelope in **Figure 7** illustrates the key proteome changes relevant to the PL-, SBF- and PBF-type growth in Mmr.

Time-kill curve analysis for indicating persister cells in maturing biofilms

As growth mode-dependent differences imply higher persistence/tolerance-associated activities in biofilms than in planktonic cultures, we next validated these findings by exposing both the planktonic and biofilm cells to rifampicin and monitored cell death using a time-kill curve analysis. This method enables the demonstration of an overall slower killing efficacy for tolerant populations or a bimodal time-kill curve that indicates the presence of a persistent bacterial subpopulation (31, 32).

First, we used a bacterial killing assay with bioluminescence as a readout to quantify the tolerance/persistence in the planktonic cultures and two-week-old biofilms. The planktonic and biofilm cells were treated with 400 μg mL^{-1} rifampicin (64 x MIC, minimum inhibitory concentration), and the rate of bacterial killing was monitored for seven days. The use of bioluminescence as a readout for killing biofilm-associated bacteria was also assessed using an OD_{600}-based method **(Fig. S3A)**. The time-kill curve for the biofilm population was bimodal, showing the faster killing of a susceptible subpopulation followed by a slower killing of a persistent subpopulation of cells (**Fig. 8A**). These results indicate that Mmr biofilms harbor significantly more persister cells than logarithmic phase planktonic populations.

Next, the development of persistence in the biofilms was monitored by killing two-day-, four-day-, and one-week-old biofilm cells with 64 x MIC rifampicin. Analysis of the time-kill curves showed that persistence increases gradually in the maturing biofilms, reaching a statistically significant increase in one-week-old biofilms compared to the planktonic cells (P = 0.0002) (**Fig. 8B)**. In untreated biofilms, the bioluminescence signal level continues to increase well past the one-week timepoint, showing that the biofilm-associated mycobacterial population is replicating and/or metabolically active at this stage **(Fig. S3B)**. This indicates that increased persistence is not (mainly) caused by the induction of

dormancy or metabolic inactivity. According to our experimental settings, PBFs form later than SBFs and are visually detectable only after two weeks. Thus, this data shows that a substantial persister subpopulation develops in SBFs by the first week of biofilm development.

To test if the formation of persister cells differs between the two biofilm subtypes, PBFs and SBFs were collected separately and tested with the time-kill assay under 64 x MIC rifampicin. After seven days, the time-kill curves indicated no significant differences in the rate of persistence between the two-week-old pellicle and submerged biofilms (P = 0.51) (**Fig. 8C**). Thus, our results indicate that the proportion of persisters is greater in over one-week-old Mmr biofilms than in logarithmic planktonic cell populations, and that the biofilm-associated persistence increases over time.

DISCUSSION

Mmr grows in morphologically distinct biofilm subtypes *in vitro*

A recent study confirmed that Mtb forms biofilm-like communities in vivo, which confers increased tolerance to rifampicin and thus provides an explanation for the chronic nature of TB (11). The present study shows that Mmr grows in two different biofilm subtypes, and that reduced CelA1 hydrolase activity is one of the main triggers of biofilm growth and increased tolerance to rifampicin in both biofilm subtypes. Studies on Mtb and *M. smegmatis* have demonstrated that cellulose filaments are vital structural constituents of mycobacterial biofilm-ECMs as well as essential for biofilm formation and the development of tolerance/persistence (9, 11, 18, 19). We also show that the Mmr biofilm subtypes show distinct morphologies, with SBFs containing lichen-like structures and PBFs consisting of ribbon-like cords under the same in vitro conditions. Biofilm growth accompanied by cording-like growth morphology is also reported for other mycobacteria and Mtb, in which

the surface interactions mediated by e.g., mycolic acids modulating the mycomembrane/capsule hydrophobicity (11, 33). The proteomic data presented here suggest that subtype-specific changes in cord-factor TDM-synthesis (mycolyltransferase Ag85), Esx1-secretion, phthiocerol dimycocerosate (PDIM) export (MmpL7), MA cyclopropanation (PcaA/Cma2), and lectin synthesis (33-37) may have affected the mycomembrane composition and thereby contributed to distinct biofilm growth morphologies in Mmr.

Mmr may use membrane vesicles to deliver proteins in the biofilm-ECM

The LFQ proteomics identified cytoplasmic proteins and proteins associated with the inner-/mycomembrane as the largest protein group in both the planktonic and biofilm cells. These findings are supported by studies identifying cytoplasmic proteins in the capsule of another Mmr strain (E11) and by showing that their number increases when mycobacterial cells grow in the biofilms, as demonstrated for *M. bovis* (17, 20). Membrane vesiculation is the most likely explanation for their presence on Mmr cells and within the biofilm-ECM, as several reports have demonstrated the presence of MVs on mycobacterial cells (38) as well as trapped in biofilm-ECMs in other bacteria (39). In addition, several of the cytoplasmic and inner-/mycomembrane-proteins detected here, including e.g., enzymes involved in cell wall synthesis and lipid/ fatty acid metabolism, were previously identified in MVs released by *Mycobacterium avium* 104 in response to starvation (40). Mycobacteria have been shown to form MVs from mycomembrane (mMV) during normal growth (cell lysis/death) and/or from inner-membrane (iMV) by blebbing in response to stress (e.g., iron-limitation and anoxia) (38). This report supports the idea that the identified myco-/inner-membrane-proteins could have also entered the biofilm-ECMs by MVs in our study. We further propose that CwlM, a N-acetylmuramoyl-L-alanine amidase (41, 42), detected

379 in one-week-old SBFs, is involved in this process, as weakening the link between the
380 mycomembrane and peptidoglycan has been suggested to stimulate MV blebbing in the
381 mycobacteria (38). Taken together, these findings may explain why more cytoplasmic
382 proteins were detected on this biofilm subtype, as the maturing biofilm cells grow under
383 reduced oxygen tension and anoxia is one of the factors able to trigger the membrane
384 vesiculation.

385 Bacterial MVs are involved in i.e., cell-cell communication, biofilm formation, virulence,
386 antibiotic resistance, iron scavenging, nutrient acquisition and modulating the host immune
387 system (43). We detected several cytoplasmic proteins involved in signal transduction
388 (e.g., PknL specific to SBFs and an adenylate cyclase detected only in biofilm-ECMs) and
389 enzymes involved in biofilm formation. GroEL1 and Fatty-Acid-Synthase system (FAS-I
390 and FAS-II) enzymes were among the detected proteins that coordinate biofilm formation
391 in mycobacteria. The GroEL1 chaperone is involved in the synthesis of mycolic acids
392 (MAs) that eventually become inserted in the mycomembrane as trehalose dimycolates
393 (TDM) and monomycolates (TMM) beneath the capsule (14, 21). This chaperone interacts
394 with ketoacyl-ACP synthase KasA (FAS-II) to modulate the synthesis of short-chain MAs
395 specifically during biofilm formation (21). A lack of GroEL1 has been reported to prevent
396 the biofilm formation and to affect the biosynthesis and composition of MAs in
397 *Mycobacterium bovis* BCG, whereas the GroEL1 deficiency blocks the formation of mature
398 biofilms in *M. smegmatis* (21, 24). In addition, the overexpression of KasA and the
399 inactivation of other FAS-II enzymes, such as enoyl-ACP reductase (InhA) and 3-oxoacyl-
400 [acyl-carrier-protein] synthase 2 (KasB), have also been reported to prevent biofilm
401 formation and formation of cords by reducing the cyclopropanation of MAs (14, 21, 25).
402 Here, GroEL1, KasA and InhA were detected as more abundant in the SBFs, implying that

these enzymes could support the initial stages of SBF-type biofilm growth, as GroEL and KasA were detected with the highest abundancies already on the two-day-old SBFs.

Although no cell lysis was seen during the sample preparation for proteomic analysis **(Table S7)**, we cannot exclude the possibility that some of the cytoplasmic or inner-/myco-membrane-proteins were released by autolysis during growth. In other Gram-positive bacteria, cytoplasmic proteins reach the extracellular space via regulated autolysis (involving autolysins/peptidoglycan hydrolases), and, as soon as the pH of the culture medium drops (due to the active metabolism of the growing cells), many of the released proteins show an enhanced ability to bind to the cell wall and biofilm-ECM structures (43-48). SBF cells are exposed to hypoxic conditions, and oxygen limitation acidifies the biofilm matrix (48), allowing for a more efficient interaction between the cytoplasmic proteins and biofilm-ECM structures. Thus, this could explain the presence of r-proteins as the largest cytoplasmic protein group already on two-day-old SBFs; the strong positive charge of these proteins has been proposed to mediate electrostatic interactions with anionic cell-surface components, which promotes cell aggregation and biofilm stabilization (48). Since the exposed mycomembranes with MAs as the major components create a condition stimulating an interaction with many cytoplasmic proteins, pH-dependent binding with the cell surface components could also explain why cytoplasmic proteins were detected on Mmr cells grown on Tween-80.

Biofilm subtypes differ in terms of secreted virulence and adhesion factors

The proteomics data indicated that the mycomembrane-associated PPE/PE family proteins were remarkably greater in number in the PL than in the PBFs or SBFs, indicating that Mmr in a single cell state could more readily interact with the host, and modulate the host immune response and/or nutrient transport (49, 50). PL cells were cultured in the

presence of Tween-80, which, in detaching the mycobacterial capsule (17), most likely helped identify these immunogens. Tween-80 can also induce alterations in the morphology, pathogenicity, and virulence of mycobacteria (51). For example, genes encoding lipases and cutinases have been shown to be significantly upregulated in Mtb in response to this nonionic surfactant. Our data is in line with this by showing that several lipases/cutinases, with a likely ability to hydrolyze Tween-80, were more abundant on PL cells compared to biofilms. As Tween-80 is considered to mimic a lipid rich milieu of macrophages (51), the detected PL-proteome changes here may reflect a metabolic adaption to conditions faced in vivo.

Our findings also suggest that Mmr uses different T7SS pathways in SBFs and PBFs for virulence and adherence. For example, the Esx1-secretion components and substrates (EsxA/B, EspB, EspF, EccA1, EspG1, EspH, EspL and MycP) were detected as more abundant in the PBFs, while those associated with the Esx5-type secretion were overall more abundant in the SBFs (Ecc, EspG, PPE/PE proteins). Both secretion pathways can contribute to virulence and subverting the host immune system in Mtb (52). The major subtype-dependent differences between the PBFs and SBFs were related to invasion and adherence, including the MCE proteins, fibronectin binding APA and HphA, which can modulate host cell signaling as well as aid adhesion or entry into host cells (53-55). All these proteins were significantly more produced on the PBFs than the SBFs, and, in the case of MCEs, may also involve MVs, as these adhesins are located on the inner membrane of the mycobacterial cell wall. HphA also has implications in promoting cell-cell aggregation in Mtb (56), suggesting that this adhesin could also contribute to cording during PBF-type growth.

Biofilm subtypes use different tolerance- and persistence-conferring mechanisms

Tolerance is defined as the extent of time that bacteria can survive in the presence of a high antibiotic concentration (31), whereas persisters are a subpopulation of phenotypically drug tolerant cells that do not grow in the presence of an antibiotic (32). We show that antibiotic killing of biofilm cells occurs at a significantly slower rate when compared to PL cells. The time-kill curve indicated the temporally increased formation of a persistent subpopulation with slower killing kinetics as well as the formation of persisters in SBFs already after one week. At this stage, Mmr biofilms remained metabolically active and replicating, indicating that persistence develops due to phenotypic differentiation during biofilm growth rather than via the induction of dormancy.

The proteomic findings suggest that Mmr could use both overlapping and subtype-specific mechanisms for increasing its tolerance and persistence, in which MVs or other non-classical routes for protein export may play a role. Here, most significant proteome changes related to cytoplasmic and inner-/mycomembrane-proteins and included enzymes/proteins involved in the TCA cycle and glyoxylate shunt, mycolic acid synthesis stress response, and energy and redox metabolisms. A recent transcriptome analysis of another non-tuberculous mycobacterial model, *Mycobacterium abscessus*, supports our findings; biofilm growth activated the glyoxylate shunt, redox metabolism and the MA synthesis-associated elongation and desaturation pathways. The TCA cycle associated enzyme CitA was recently reported to control the asymmetric cell division in *Caulobacter crescentus* (57). This process has been shown to lead to the formation of heterogenous cell populations in biofilms, macrophages, and granulomatous lesions also in mycobacteria (7, 58, 59). Here, our findings indicated the presence of this enzyme on one-week-old SBFs, suggesting that the asymmetric cell division occurs before the PBFs are formed. Moreover, arabinosyltransferases EmbA and EmbB, involved in the polymerization of the

arabinogalactan, were also detected with high abundances in SBFs by one week onward, suggesting that strengthening the arabinogalactan could further help residing cells, including the persisters, increase their tolerance to rifampicin, as demonstrated with Mtb persisters under hypoxia (60). Taken together, these findings strengthen the hypothesis that persisters are indeed formed in one-week-old SBFs, and supports the results obtained with the biofilm killing assay on the SBFs at this time point.

We also suggest that cells in PBFs use different TCA cycle enzymes, such as aconitase (ACN), malate dehydrogenase (MDH), enolase (ENO), and/or fructose-bisphosphate aldolase (FBA), to maintain long-term survival. In other gram-positive bacteria these enzymes belong to known moonlighting proteins with established secondary roles outside of the bacterial cell (e.g., adhesion)(30). In mycobacteria, these enzymes have been reported to contribute to increased viability or persistence (61-63). The associated glyoxylate shunt could also be involved (64), as isocitrate lyase 1 (ICL1) was detected as more abundant on the SBFs, implying that this enzyme could help residing cells increase their antioxidant defense and antibiotic tolerance (65). In contrast, ICL2 was produced more on the PBFs, which may help the cells to survive under starvation conditions when fatty acids are used as the primary carbon source (66). This is in line with the temporally increased production of diacylglycerol *O*-acyltransferase (Tgs1) in PBFs, which can promote the accumulation of triacylglycerols (TAGs); a process that has been considered a hallmark feature of persisting Mtb/latent TB and a long-term energy source for Mtb and have been found in substantial amounts in the mycobacterial cell wall (67, 68). The detection of trehalase as significantly more abundant in four- to 12-week-old PBFs, strengthens the idea that cells within this biofilm subtype suffer from nutrient stress and activate trehalose salvage/recycling to promote redox and energy homeostasis, as seen under carbon limitations in Mtb (69). These findings may also explain the detection of

503 proteases, chaperones, and assisting stress-proteins in high numbers in the biofilm-ECMs,
504 including e.g., the proteases Clp/Lon and the cold-shock protein CpsD, with known
505 implications in stringent response, persistence and/or post-antibiotic recovery (70-72).
506 These proteins were detected here as more abundant in the PBFs than in the SBFs,
507 implying that these pathways are preferred in PBFs to maintain viability.
508 A recent study comparing high numbers of persister Mtb mutants using genomics and
509 transcriptomics indicated a significant upregulation of energy production pathways and
510 pathways involved in redox reactions (oxidoreductase) (73). The ECM-proteome changes
511 occurring during SBF-type growth are in line with this report, as the components of the
512 respiratory electron transfer chain (cytochrome bc1 complex, cytochrome c terminal
513 oxidase, and F0F1-ATPase synthase) were detected as more abundant on the SBFs
514 facing more hypoxic conditions than the PBFs. Our findings also agree with previous
515 reports showing that the electron transfer chain is essential for maintaining ATP
516 homeostasis and the viability of nonreplicating/persistent Mtb cells under hypoxia (74-76).
517 In addition, we show that both redox and iron metabolism could also play a biofilm
518 subtype-specific role in helping the cells cope with hypoxia/aeration-related stress (77);
519 several oxidoreductases, thioredoxin and a superoxide dismutase (SOD) were overall
520 more abundant in the SBFs, and a catalase-peroxidase (KatG) and alkyl
521 hydroxyperoxidases (AhpCF) as more abundant in the PBFs. These enzymes have been
522 shown to protect Mtb against oxidative stress by the reduction of superoxide radicals into
523 less toxic intermediates for inhibiting autophagy, apoptosis and cellular damage (78). Iron
524 storing proteins ferritin (BfrB) and bacterioferritin (BfrA) can confer increased redox
525 resistance on Mtb and protect the cells against oxidative stress and hypoxia, respectively
526 (79). Here, these iron storing proteins displayed biofilm subtype-specific abundance

527 changes, implying that SBFs could rely on BfrB to cope with hypoxia and PBFs on BrfA to
528 help cells grow at the air–liquid interface.
529
530 **CONCLUSIONS**
531 The present study reports an in-depth view of ECM-proteome changes occurring in Mmr
532 ATCC927 during biofilm growth in vitro from two days to three months. We show that this
533 non-tuberculous mycobacterial model forms SBFs already after two days, whereas the
534 formation of detectable PBFs was observed after two weeks of growth in the absence of
535 Tween-80. Both biofilm subtypes were formed physically under the same conditions with
536 clearly distinct growth morphologies: SBFs with lichen-like structures and PBFs with
537 ribbon-like cords. We show that the reduced CelA1-mediated cellulose hydrolysis is
538 necessary to establish proper biofilm growth, growth morphology and increased tolerance
539 to rifampicin for both biofilm subtypes. The formation of persisters in both biofilm subtypes
540 and increased tolerance was further confirmed by the newly established bioluminescence-
541 based time-kill assay, which provides an effective tool for quantifying tolerance and
542 persistence in Mmr. The proteomic findings imply that subtype-dependent changes in the
543 MA synthesis and modification, Esx1-type secretion, and the production of specific
544 adhesins were the major drivers of distinct biofilm growth morphologies. We also propose
545 that pathways associated with MA biosynthesis, development of tolerance/persistence and
546 oxidative/redox stress are differentially used in PBFs and SBFs to maintain prolonged
547 viability. Possible explanations for these differences include the different oxygen tensions
548 encountered by the biofilm subtypes, differences in membrane vesiculation activities
549 and/or other non-classical pathways for protein export. Taken together, this is the first
550 study reporting on ECM-proteome dynamics in maturing mycobacterial biofilms and
551 predicting biofilm subtype-specific changes in cell-cell communication, biofilm matrix

552 formation, virulence, and tolerance/persistence. This is also the first time that the kinetics
553 of persistence have been explicitly measured from mycobacterial biofilms.
554
555 **MATERIALS AND METHODS**
556 **Preparing bacterial cells for surface proteomics**
557 *Mycobacterium marinum* (ATCC 927) with the pTEC27 plasmid expressing the red
558 fluorescent protein tdTomato (Addgene #30182, http://n2t.net/addgene:30182) (29) was
559 pre-cultured on Middlebrook 7H10 plates with 10% (v/v) Oleic Albumin Dextrose Catalase
560 (OADC) enrichment (Fisher Scientific, NH, USA) and 0.5% (v/v) glycerol at 29 °C for one
561 week. For planktonic cultures, an inoculum of Mmr was transferred into a Middlebrook 7H9
562 medium supplemented with 10% (v/v) ADC (Fisher Scientific, NH, USA), 0.2% (v/v)
563 glycerol, and 0.2% (v/v) Tween-80 (Sigma-Aldrich, MO, USA), and the cells were cultured
564 at 29 °C in cell culture flasks with filter caps. After three days of incubation the cell cultures
565 were diluted to obtain an OD_{600} of 0.042 and the dilutions were cultured for an additional
566 2 days at +29 °C until harvesting. For the biofilm cultures, a Middlebrook 7H9 medium with
567 the ADC growth supplement but without Tween-80 or glycerol was used. The inoculum
568 was cultured for three days at +29 °C until the OD_{600} reached 0.45. The cell cultures were
569 diluted 1:40, and the dilutions were divided into 10 ml aliquots. The cap of each tube was
570 sealed with Parafilm M® laboratory wrapping film, and the cultures were incubated at +29
571 °C. Planktonic and biofilm cell samples (SBFs and PBFs separately) were collected at the
572 time points indicated in **Figure 2A**. All the cultures were performed in quadruplicates.
573 Planktonic cells were harvested by centrifugation (3 min, 5 000g, +4 °C) and the pelleted
574 cells were suspended gently in ice-cold buffer (100 mM Bis-Tris, pH 6.5) to remove
575 interfering/non-specifically bound proteins. This step prevents the detachment/removal of
576 cytoplasmic moonlighters bound to the cell surfaces/biofilm-ECM (43-46, 79, 80). The

PBFs were collected with an inoculation loop, the extra medium was removed by pipetting to avoid cross-biofilm type contamination, and the SBFs were harvested by pipetting/scraping. The PBFs and SBFs were collected in separate Eppendorf tubes the ice-cold buffer (100 mM Bis-Tris, pH 6.5). Cells (planktonic and biofilm cultures) were pelleted by centrifugation (3 min, 5 000*g*, +4 °C) and the washed cells were suspended gently in 95 µL of 100 mM TEAB (triethylammonium bicarbonate, pH 8.5) for the enzymatic shaving reaction.

Trypsin/Lys-C shaving of planktonic and biofilm cells

Peptides from cell-surface/biofilm-ECM-associated proteins were released via a Trypsin/Lys-C mix (Promega) at a final concentration of 50 ng μL^{-1}, and the digestions were incubated at 37 °C for 20 minutes. The method was validated by counting the number of colonies formed on the planktonic/single and biofilm cells treated with/without the enzyme mix **(Table S7)**. The released peptides and the enzymes were recovered by filtration through a 0.2 µm acetate membrane (Costar® Spin-X Centrifuge Tube Filter, Corning Inc., Corning, NY, US) by centrifugation (8000*g*, 3 min, 20 °C). Flow-troughs were incubated for 16 hours at 37 °C. The concentration of released peptides in each sample was measured with a NanoDrop2000 spectrophotometer (Thermo Scientific). Digestions were terminated with 0.6% (v/v) trifluoroacetic acid (TFA) (Sigma Aldrich) and the peptides were purified using ZipTip C18 (Millipore) according to the manufacturer's instructions and dried using a miVac centrifugal vacuum concentrator (GeneVac).

LC-MS/MS analysis

The peptides were dissolved in 0.1% (v/v) formic acid (FA) and analyzed with nanoLC-MS/MS using an Easy-nLC 1000 nano-LC system (Thermo Scientific) coupled with a

602 quadrupole Orbitrap mass spectrometer (Q Exactive^{TM}, ThermoElectron, Bremen,
603 Germany) as previously reported (80). The obtained MS raw data was processed via
604 MaxQuant software (version v.1.6.1.0) with the built-in search engine, Andromeda (81,
605 82), using a protein database comprising all 5,564 Mmr protein sequences (Uniprot
606 proteome: up000257451, genome accession: PEDF01000000) both forward and reverse.
607 Carbamidomethyl (C) was set as a fixed and methionine oxidation was set as a variable
608 modification. Tolerance was set to 20 ppm in the first search and 4.5 ppm in the main
609 search. Trypsin without the proline restriction enzyme option and with two allowed
610 miscleavages was used. The minimal unique plus+ razor peptide number was set to 1; the
611 FDR was set to 0.01 (1%) for peptide and protein identification; and LFQ with default
612 settings was used. The mass spectrometry proteomics was deposited in the
613 ProteomeXchange Consortium via the PRIDE (83) partner repository with the dataset
614 identifier PXD02010.
615
616 **Proteome statistics and bioinformatics**
617 The identified Mmr proteins were manually curated by characterizing hypothetical and
618 tentatively annotated proteins with the aid of the Basic Local Alignment Search Tool
619 (BLAST) program from the National Center for Biotechnology Information (NCBI) (84-86),
620 combined with CDD/SPARCLE conserved domain identification (87) and SmartBLAST
621 (UniProt) searches. General protein functions were annotated using the Gene Ontology
622 (GO) database (88). Isoelectric points (pIs) and molecular weights (MWs) for the identified
623 proteins were predicted using EMBOSS Pepstats (89) at https://www.ebi.ac.
624 uk/Tools/seqstats/emboss_pepstats/. The presence of possible protein secretion motifs
625 (classical and nonclassical) for all the predicted and identified proteins was obtained with
626 SignalP4.1 (90) (http://www.cbs.dtu.dk/services/SignalP/) and SecretomeP 2.0/SecP (91)

627 (http://www.cbs.dtu.dk/services/SecretomeP/). The presence of transmembrane spanning
628 domains/helices (TMDs) was determined with the TMHMM Server v. 2.0 at http://www.cbs.
629 dtu.dk/services/TMHMM/ (92, 93) for the identified proteins.
630 For indicating statistically significant abundance changes the log2-transformed LFQ data
631 was analyzed in Perseus v.1.6.2.3 (94) using a Student's *t*-test with permutation-based
632 FDR adjustment. For the multivariate analyses, the missing values were replaced by
633 imputed values from the normal distribution (width = 0.3, down shift = 1.8) and then
634 normalized (z-score) prior to ANOVA for multi-sample testing (S0 set to 0.1 and a
635 permutation-based FDR of 5%) and hierarchical clustering/PCA. STRING Protein
636 Interaction Network and Functional Enrichment Analyses (GO, KEGG, InterPro, Pham)
637 were studied using the STRING database v. 11 (95). Interaction scores were set to high
638 (0.700) confidence, and the interacting proteins were clustered using Markov clustering
639 (MCL) with the inflation parameter set to 4.0–6.0. Functional enrichments were statistically
640 assessed with both rank- and gene set-based approaches (FDR of 0.05).
641
642 **Creation of the CelA1 overexpression construct in Mmr**
643 The Mmr CelA1 overexpression strain was created by ordering the MMAR_0107 open
644 reading frame in the pUC57 vector with appropriate restriction sites from GenScript and
645 subcloning the construct into the pTEC27 vector (AddGene) (29), which carryies the red
646 fluorescent protein tdTomato. The sequence of the plasmid was confirmed by sequencing.
647 The resulting plasmid was transformed into an electrocompetent Mmr ATCC927 strain.
648 Transformants were selected on Middlebrook 7H10 agar plates containing 10% (v/v)
649 OADC enrichment, 0.5% (v/v) glycerol and 75 µg mL^{-1} hygromycin.
650
651

652 **RNA and DNA extractions**

653 For RNA and DNA extractions, the *CelA1* overexpression strain and Mmr were precultured
654 on MiddleBrook 7H10 plates and transferred into the Middlebrook 7H9 medium described
655 above (75 µg mL^{-1} hygromycin for the CelA1 strain). After three days, the bacterial cells
656 were harvested, pelleted, and homogenized in TRI Reagent (Thermo Fisher Scientific, NH,
657 USA) with ceramic beads using the PowerLyzer24 (Mobio, CA, USA). After
658 homogenization, the samples were sonicated for nine minutes and the RNA and DNA
659 were extracted according to the manufacturer's instructions.

660

661 ***CelA1* expression and the quantification of mycobacterial loads by qPCR**

662 Prior to qPCR analysis, RNA was reverse transcribed into cDNA with a Reverse
663 Transcription kit (Fluidigm, CA, USA) according to the manufacturer's instructions. *CelA1*
664 expression was measured using soFast EvaGreen Supermix with the Low ROX qPCR kit
665 (Bio-Rad, CA, USA) and the CFX96 qPCR system (Bio-Rad, CA, USA). The primers used
666 for *CelA1* were: (forward: 5'- ACACTCCGCAGTCCTACT-3' and reverse: 5'- TAGAGCGTC
667 AGAATCGGC-3'). The number of mycobacterial cells in the sample was quantified using
668 the SensiFAST SYBR No-ROX qPCR kit (Bioline, London, UK) on bacterial DNA
669 according to the manufacturer's instructions. The primers used for Mmr quantification were
670 targeted against 16S-23S, locus AB548718 (forward: 5'- CACCACGAGAAACACTCCAA-3'
671 and reverse: 5'- CACCACGAGAAACACTCCAA-3'). Each bacterial quantification qPCR
672 run included a standard curve of the known amounts of Mmr DNA. The mycobacterial cell
673 number in each sample was used to normalize the *CelA1* expression.

674

675

676

677 **Widefield deconvolution microscopy (WDeM) of Mmr biofilms**

678 PBFs and SBFs formed by Mmr with pTEC27 (WT), expressing the red fluorescent protein
679 tdTomato (29), and Mmr overexpressing CelA1 were prepared as follows. Briefly, the cells
680 were incubated at 29 °C and the surface-attached cells were imaged at seven, 14 and 21
681 days after dilution. In situ imaging of the SBFs was conducted with Nikon FN1 upright
682 epifluorescence microscope equipped with 20x/0.8 dry objective, Hamamatsu ORCA-
683 Flash4.0 V3 Digital CMOS camera and CoolLED pE-4000 light source. tdTomato was
684 excited with 550 nm LED and fluorescence was collected with 617/73 band-pass emission
685 filter. Image stack were collected with 2µm intervals (x-y pixel size 325 nm). The data was
686 deconvolved with Huygens Essential deconvolution software (SVI, Amsterdam,
687 Netherlands) using 200 iteration limit, signal-to-noise ratio of 30 and quality threshold of
688 0.01.

689

690 **Biofilm tolerance assays**

691 The role of CelA1 overexpression in the antibiotic tolerance of Mmr was assessed as
692 follows. First, the *CelA1* overexpression strain and pTEC27 control strain were cultured
693 for one week on 7H10 plates (10% OADC, 0.5% glycerol + 75 µg mL^{-1} hygromycin) and
694 then transferred in a Middlebrook 7H9 medium supplemented with 10% ADC and 75 µg
695 mL^{-1} hygromycin) at an OD_{600} of 0.1 to initiate biofilm growth. Aliquots of bacterial
696 suspension (192 µl of per well) were added to 96-well-plates in triplicate, sealed with
697 parafilm and incubated at +29 °C in the dark. Planktonic cultures grown in the presence of
698 0.2% glycerol were used as controls. Eight µl of antibiotics per well was added two, four,
699 seven and 14 days after the start of the liquid culture. The final antibiotic concentrations
700 used were 400, 100, 25 and 6.25 µg mL^{-1} for the Rifampicin TOKU-E solution. Untreated
701 wells were used as controls. Ten µl per sample was plated on 7H9 plates (10% OADC, 75

µg mL^{-1} hygromycin) one week after the addition of antibiotics. The plates were incubated at +29 °C for seven to nine days and the colonies were counted.

Biofilm persistence assays

Mmr (ATCC 927) with a bioluminescence cassette in the pMV306hsp+LuxG13 plasmid was used for antibiotic tolerance assays. pMV306hsp+LuxG13 was provided by Brian Robertson and Siouxsie Wiles (Addgene plasmid #26161; http://n2t.net/addgene: 26161). To measure the kinetics of bacterial killing, the bioluminescent Mmr strain was first cultured on Middlebrook 7H10 agar (Sigma-Aldrich) supplemented with 0.5% (v/v) glycerol (Sigma-Aldrich) and 10% (v/v) OADC enrichment (BD, Becton Dickinson) at 29 °C for seven days in the dark. To initiate biofilm formation, the Mmr cells were suspended in Middlebrook 7H9 broth (Sigma-Aldrich) supplemented with 10% (v/v) ADC enrichment (BD, Becton Dickinson) at a starting OD_{600} of 0.1. Planktonic cultures were prepared in the same way except that the medium contained 0.2% (v/v) glycerol (Sigma-Aldrich) and 0.2% (v/v)Tween-80 (Sigma-Aldrich). Bacterial suspensions (192 µL per well in triplicates) were divided on to white 96-well plates (Perkin Elmer). The biofilm cultures were sealed with laboratory film and incubated at 29 °C in the dark to the desired ages. Rifampicin solution (TOKU-E) in water at a final concentration of 400 µg mL^{-1} corresponding to 64 x MIC (minimum inhibitory concentration) was added to the bacterial suspensions and incubated for seven days at 29 °C in the dark. The bioluminescence signal was measured with an EnVision plate reader (Perkin Elmer) as a readout for bacterial survival three times for three seconds per well daily from a white 96-well plate for seven days. The background signal from media only wells was first subtracted from the sample wells and an average of the three measurements normalized with the starting bioluminescence signal was used to

draw time-kill curves of the bacterial population in the biofilms at different maturation stages.

To compare the level of persistence/tolerance in the PBFs and SBFs, Mmr was cultured in a total volume of 10ml at the starting OD_{600} value of 0.1. After two weeks, the biofilms were collected separately from the tubes by lifting the pellicle with a 1-µL inoculation loop coupled with careful pipetting. The pellicle and submerged biofilms were centrifuged at 10,000*g* for three minutes, the supernatants were collected, and the wet weight of the bacterial mass was measured. The bacterial cells were suspended into previously collected spent media at the concentration of 15 mg mL^{-1}, vortexed briefly, and divided on white 96-well plates (Perkin Elmer) with 192 µL of cell suspension per well in triplicate. Eight µl of TOKU-E solution at a final concentration of 400 µg mL^{-1} were pipetted on the bacterial suspension. Liquid cultures were incubated for seven days at 29 °C in the dark and the bioluminescence signal was measured daily with an EnVision plate reader (Perkin Elmer) three times for three seconds per well. The background signal from the media-only wells was first subtracted from the sample wells, and an average of the three measurements was normalized with the starting bioluminescence signal measured just before adding the rifampicin. The statistical significance of the differences between the time-kill curves was tested with a log-rank test using Prism5 software (GraphPad).

ACKNOWLEDGEMENTS

The financial support of the Academy of Finland (projects no. 322010 (AF, JYK, MP) and 326674 (MP), Jane and Aatos Erkko Foundation (MP), Sigrid Jusélius Foundation (MP), Foundation of the Finnish Anti-Tuberculosis Association (Suomen Tuberkuloosin Vastustamisyhdistyksen Säätiö)(HL, LMV, KS) and Tampere Tuberculosis Foundation (MP, KS, HM, HL, LMV) is greatly appreciated. Mass spectrometry-based proteomic

analyses were performed by the Proteomics Core Facility, Department of Immunology, University of Oslo/Oslo University Hospital, which is supported by the Core Facilities program of the South-Eastern Norway Regional Health Authority. This core facility is also a member of the National Network of Advanced Proteomics Infrastructure (NAPI), which is funded by the Research Council of Norway INFRASTRUKTUR-program (project number: 295910)(TAN).

REFERENCES

1. Global tuberculosis report 2020. Geneva: World Health Organization; 2020. Licence: CC BY-NC-SA 3.0 IGO.

2. Panjabi R, Comstock GW, Golub JE. 2007. Recurrent tuberculosis and its risk factors: adequately treated patients are still at high risk. Int J Tuberc Lung D 11:828-837.

3. Rosser A, Marx FM, Pareek M. 2018. Recurrent tuberculosis in the pre-elimination era. Int J Tuberc Lung D 22:139-150.

4. Aldridge BB, Fernandez-Suarez M, Heller D, Ambravaneswaran V, Irimia D, Toner M, Fortune SM. 2012. Asymmetry and aging of mycobacterial cells lead to variable growth and antibiotic susceptibility. Science 335:100-104.

5. Malherbe ST, Shenai S, Ronacher K, Loxton AG, Dolganov G, Kriel M, Van T, Chen RY, Warwick J, Via LE, Song T, Lee M, Schoolnik G, Tromp G, Alland D, Barry CE, 3rd, Winter J, Walzl G, Catalysis TBBC, Lucas L, Spuy GV, Stanley K, Thiart L, Smith B, Du Plessis N, Beltran CG, Maasdorp E, Ellmann A, Choi H, Joh J, Dodd LE, Allwood B, Koegelenberg C, Vorster M, Griffith-Richards S. 2016. Persisting positron emission tomography lesion activity and *Mycobacterium tuberculosis* mRNA after tuberculosis cure. Nat Med 22:1094-1100.

6. Jankute M, Cox JA, Harrison J, Besra GS. 2015. Assembly of the Mycobacterial cell wall. Annu Rev Microbiol 69:405-423.

7. Sarathy JP, Via LE, Weiner D, Blanc L, Boshoff H, Eugenin EA, Barry CE, 3rd, Dartois VA. 2018. Extreme drug tolerance of *Mycobacterium tuberculosis* in caseum. Antimicrob Agents Chemother 62:e02266-17.

8. Basaraba RJ, Ojha AK. 2017. Mycobacterial biofilms: Revisiting tuberculosis bacilli in extracellular necrotizing lesions. Microbiol Spectr 5:10.1128/microbiolspec.TBTB2-0024-2016.

9. Chakraborty P, Bajeli S, Kaushal D, Radotra BD, Kumar A. 2021. Biofilm formation in the lung contributes to virulence and drug tolerance of *Mycobacterium tuberculosis*. Nat Commun 12:1606.

10. Handwerger S, Tomasz A. 1985. Antibiotic tolerance among clinical isolates of bacteria. Annu Rev Pharmacol Toxicol 25:349-380.

11. Chakraborty P, Kumar A. 2019. The extracellular matrix of mycobacterial biofilms: could we shorten the treatment of mycobacterial infections? Microb Cell 6:105-122.

12. Marrakchi H, Laneelle MA, Daffe M. 2014. Mycolic acids: structures, biosynthesis, and beyond. Chem Biol 21:67-85.

13. Flemming HC, Wingender J, Szewzyk U, Steinberg P, Rice SA, Kjelleberg S. 2016. Biofilms: an emergent form of bacterial life. Nat Rev Microbiol 14:563-575.

14. Ojha AK, Baughn AD, Sambandan D, Hsu T, Trivelli X, Guerardel Y, Alahari A, Kremer L, Jacobs WR Jr, Hatfull GF. 2008. Growth of *Mycobacterium tuberculosis* biofilms containing free mycolic acids and harbouring drug-tolerant bacteria. Mol Microbiol 69:164-174.

800 **15.** Caceres N, Vilaplana C, Prats C, Marzo E, Llopis I, Valls J, Lopez D, Cardona P-J,
801 2013. Evolution and role of corded cell aggregation in *Mycobacterium tuberculosis*
802 cultures. Tuberculosis 93:1-9.
803 **16.** Kalsum S, Braian C,1 Koeken VACM, Raffetseder J, Lindroth M, van Crevel R, Lerm
804 M. 2017. The cording phenotype of *Mycobacterium tuberculosis* induces the
805 formation of extracellular traps in human macrophages. Front Cell Infect Microbiol
806 7:278.
807 **17.** Sani M, Houben EN, Geurtsen J, Pierson J, de Punder K, van Zon M, Wever B,
808 Piersma SR, Jiménez CR, Daffé M, Appelmelk BJ, Bitter W, van der Wel N, Peters
809 PJ. 2010. Direct visualization by cryo-EM of the mycobacterial capsular layer: a labile
810 structure containing ESX-1-secreted proteins. PLoS Pathog 6:e1000794.
811 **18.** Trivedi A, Mavi PS, Bhatt D, Kumar A. 2016. Thiol reductive stress induces cellulose-
812 anchored biofilm formation in *Mycobacterium tuberculosis*. Nat Commun 7:11392.
813 **19.** Van Wyk N, Navarro D, Blaise M, Berrin J-G, Henrissat B, Drancourt M, Kremer L.
814 2017. Characterization of a mycobacterial cellulase and its impact on biofilm- and
815 drug-induced cellulose production. Glycobiology 27:392–399.
816 **20.** Pagani TD , Guimarães ACR , Waghabi MC , Corrêa PR, Kalume DE, Berrêdo-Pinho
817 M, Degrave WM, Mendonça-Lima L. 2019. Exploring the potential role of
818 moonlighting function of the surface-associated proteins from *Mycobacterium bovis*
819 BCG Moreau and Pasteur by comparative proteomic. Front Immunol 10:716.
820 **21.** Ojha A, Anand M, Bhatt A, Kremer L, Jacobs WR, Jr., Hatfull GF. 2005. GroEL1: a
821 dedicated chaperone involved in mycolic acid biosynthesis during biofilm formation in
822 mycobacteria. Cell 123:861-873.

823 **22.** McNamara M, Tzeng S-C, Maier C, Wu M, Bermudez LE. 2013.Proteome Sci.
824 Surface-exposed proteins of pathogenic mycobacteria and the role of Cu-Zn
825 superoxide dismutase in macrophages and neutrophil survival. 11: 45.
826 **23.** McNamara, M, Tzeng S-C,, Maier C, Zhang L, Bermudez LE. 2012. Surface
827 proteome of *Mycobacterium avium* subsp. *hominissuis* during the early stages of
828 macrophage infection. Infect Immun. 80:1868-1880.
829 **24.** Wang XM, Lu C, Soetaert K, S'Heeren C, Peirs P, Lanéelle MA, Lefèvre P, Bifani P,
830 Content J, Daffé M, et al. 2011. Biochemical and immunological characterization of a
831 cpn60.1 knockout mutant of *Mycobacterium bovis* BCG. Microbiology 157:1205-
832 1219.
833 **25.** Bhatt A, Fujiwara N, Bhatt K, Gurcha SS, Kremer L, Chen B, Chan J, Porcelli SA,
834 Kobayashi K, Besra GS, Jacobs WM Jr. 2007. Deletion of *kasB* in *Mycobacterium*
835 *tuberculosis* causes loss of acid-fastness and subclinical latent tuberculosis in
836 immunocompetent mice. Proc Natl Acad Sci U S A 104:5157-5162.
837 **26.** Luukinen H, Hammaren MM, Vanha-Aho LM, Parikka M. 2018. Modeling tuberculosis
838 in *Mycobacterium marinum* infected adult zebrafish. J Vis Exp 8:58299.
839 **27.** Parikka M, Hammarén MM, Harjula SK, Halfpenny 754 NJ, Oksanen KE, Lahtinen
840 MJ, Pajula ET, Iivanainen A, Pesu M, Rämet M. 2012. *Mycobacterium marinum*
841 causes a latent infection that can be reactivated by gamma irradiation in adult
842 zebrafish. PloS Pathog 8:e1002944.
843 **28.** Tobin DM, Ramakrishnan L. 2008. Comparative pathogenesis of *Mycobacterium*
844 *marinum* and *Mycobacterium tuberculosis*. Cell Microbiol 10:1027-760.
845 **29.** Takaki K, Davis JM, Winglee K, Ramakrishnan L. 2013. Evaluation of the
846 pathogenesis and treatment of *Mycobacterium marinum* infection in zebrafish. Nat
847 Protoc 8:1114-11124.

848 **30.** Chen C, Liu H, Zabad S, Rivera N, Rowin E, Hassan M, Gomez De Jesus SM, Llinás
849 Santos PS, Kravchenko K, Mikhova M, Ketterer S, Shen A, Shen S, Navas E, Horan
850 B, Raudsepp J, Jeffery C. 2021. MoonProt 3.0: an update of the moonlighting
851 proteins database. Nucleic Acids Res 49(D1):D368-D372.
852 **31.** Brauner A, Shoresh N, Fridman O, Balaban NQ. 2017. An Experimental framework
853 for quantifying bacterial tolerance. Biophys J **112:**2664-2671.
854 **32.** Brauner A, Fridman O, Gefen O, Balaban NQ. 2016. Distinguishing between
855 resistance, tolerance and persistence to antibiotic treatment. Nat Rev Microbiol
856 14:320-330.
857 **33.** Glickman MS, Cox JS, Jacobs WR Jr. 2000. A novel mycolic acid cyclopropane
858 synthetase is required for cording, persistence, and virulence of *Mycobacterium*
859 *tuberculosis*. Mol Cell 5:717-727.
860 **34.** Anton V, Rougé P, Daffé M. 1996. Identification of the sugars involved in
861 mycobacterial cell aggregation. FEMS Microbiol Lett 144:167–170.
862 **35.** Glickman MS, Cahill SM, Jacobs WR Jr. 2001. The *Mycobacterium tuberculosis*
863 *cmaA2* gene encodes a mycolic acid trans-cyclopropane synthetase. J Biol Chem
864 276:2228-33.
865 **36.** Warrier T, Tropis M, Werngren J, Diehl A, Gengenbacher M, Schlegel B, Schade M,
866 Oschkinat H, Daffe M, Hoffner S, Eddine AN, Kaufmann SHE. 2012. Antigen 85C
867 Inhibition restricts *Mycobacterium tuberculosis* growth through disruption of cord
868 factor biosynthesis. Antimicrob Agents Chemother 56:1735–1743.
869 **37.** Lerner TR, Queval CJ, Lai RP, Russell MRG, Fearns A, Greenwood DJ, Collinson L,
870 Wilkinson RJ, Gutierrez MG. 2020. *Mycobacterium tuberculosis* cords within
871 lymphatic endothelial cells to evade host immunity. JCI Insight 5:e136937.

872 **38.** Nagakubo T, Tahara YO, Miyata M, Nomura N, Toyofuku M. 2021. Mycolic acid-
873 containing bacteria trigger distinct types of membrane vesicles through different
874 routes. iScience 24:102015.
875 **39.** Schooling SR, and Beveridge TJ. 2006. Membrane vesicles: an overlooked
876 component of the matrices of biofilms. J Bacteriol 188:5945–5957.
877 **40.** Chiplunkar SS , Silva CA, Bermudez LE, Danelishvili L. 2019. Characterization of
878 membrane vesicles released by *Mycobacterium avium* in response to environment
879 mimicking the macrophage phagosome. Future Microbiol 14:293-313.
880 **41.** Deng LL, Humphries DE, Arbeit RD, Carlton LE, Smole SC, Carroll JD. 2005.
881 Identification of a novel peptidoglycan hydrolase CwlM in *Mycobacterium*
882 *tuberculosis*. Biochim Biophys Acta 1747:57-66.
883 **42.** Wang C, Zhang Q, Tang X, An Y, Li S, Xu H, Li Y, Wang X, Luan W, Wang Y, Liu M,
884 Yu L. 2019. Effects of CwlM on autolysis and biofilm formation in *Mycobacterium*
885 *tuberculosis* and *Mycobacterium smegmatis*. Int J Med Microbiol 309:73-83.
886 **43.** Antikainen J, Kuparinen V, Lähteenmäki K, Korhonen TK. 2007. pH-dependent
887 association of enolase and glyceraldehyde-3-phosphate dehydrogenase of
888 *Lactobacillus crispatus* with the cell wall and lipoteichoic acids. J Bacteriol 189:4539-
889 4543.
890 **44.** Kainulainen V, Loimaranta V, Pekkala A, Edelman S, Antikainen J, Kylväjä R,
891 Laaksonen M, Laakkonen L, Finne J, Korhonen TK. 2012. Glutamine synthetase and
892 glucose-6-phosphate isomerase are adhesive moonlighting proteins of *Lactobacillus*
893 *crispatus* released by epithelial cathelicidin LL-37. J Bacteriol 194:2509-2519.
894 **45.** Foulston L, Elsholz AKW, DeFrancesco AS, Losick R. 2014. The extracellular matrix
895 of *Staphylococcus aureus* biofilms comprises cytoplasmic proteins that associate with
896 the cell surface in response to decreasing pH. mBio 5:e01667-14.

897 **46.** Dengler V, Foulston L, DeFrancesco AS, Losick R. 2015. An electrostatic net model
898 for the role of extracellular DNA in biofilm formation by Staphylococcus aureus. J
899 Bacteriol 197:3779-3787.
900 **47.** Ebner P, Götz F. 2019. Bacterial excretion of cytoplasmic proteins (ECP):
901 Occurrence, mechanism, and function. Trends Microbiol 27:176-187.
902 **48.** Graf AC, Leonard A, Schäuble M, Rieckmann LM, Hoyer J, Maass S, Lalk M,
903 Becher D, Pané-Farré J, Riedel K. 2019. Virulence factors produced by
904 *Staphylococcus aureus* biofilms have a moonlighting function contributing to biofilm
905 integrity. Mol Cell Proteomics 18:1036-1053
906 **49.** Qian J, Chen R, Wang H, Zhang X. 2020. Role of the PE/PPE family in host–
907 pathogen interactions and prospects for anti-tuberculosis vaccine and diagnostic tool
908 design. Front Cell Infect Microbiol 10:594288.
909 **50.** Wang Q, Boshoff HIM, Harrison JR, Ray PC, Green SR, Wyatt PG, Barry CE 3rd.
910 2020. PE/PPE proteins mediate nutrient transport across the outer membrane of
911 *Mycobacterium tuberculosis*. Science 367:1147-1151.
912 **51.** Pietersen R-D, du Preez I, Loots DT, van Reenen N, Beukes D, Leisching G, Baker
913 B. 2020. Tween 80 induces a carbon flux rerouting in *Mycobacterium tuberculosis.* J
914 Microbiol Methods 170:105795.
915 **52.** Gröschel MI, Sayes F, Simeone R, Majlessi L, Brosch R. 2016. ESX secretion
916 systems: mycobacterial evolution to counter host immunity. Nat Rev Microbiol
917 14:677-691.
918 **53.** Schorey JS, Li Q, McCourt DW, Bong-Mastek M, Clark-Curtiss JE, Ratliff TL, Brown
919 EJ. 1995. A *Mycobacterium leprae* gene encoding a fibronectin binding protein is
920 used for efficient invasion of epithelial cells and Schwann cells. Infect Immun
921 63:2652-2657.

922 **54.** Fenn K, Wong CT, Darbari VC. 2020. *Mycobacterium tuberculosis* Uses Mce proteins
923 to interfere with host cell signaling. Front Mol Biosci 6:149.
924 **55.** Vinod V, Vijayrajratnam S, Vasudevan AK, Biswas R. 2020. The cell surface
925 adhesins of Mycobacterium tuberculosis. Microbiol Res 232:126392.
926 **56.** Delogu G, Brennan MJ. 1999. Functional domains present in the mycobacterial
927 hemagglutinin, HBHA. J Bacteriol 181:7464-7469.
928 **57.** Berge M, Pezzatti J, Gonzalez-Ruiz V, Degeorges L, Mottet-Osman G, Rudaz S,
929 Viollier PH. 2020. Bacterial cell cycle control by citrate synthase independent of
930 enzymatic activity. Elife 9:e52272.
931 **58.** Rego EH, Audette RE, Rubin EJ. 2017. Deletion of a mycobacterial divisome factor
932 collapses single-cell phenotypic heterogeneity. Nature 546:153-157.
933 **59.** Kieser KJ, Rubin EJ. 2014. How sisters grow apart: mycobacterial growth and
934 division. *Nat Rev Microbiol* **12:**550-562. doi:10.1038/nrmicro3299.
935 **60.** Jakkala K, Ajitkumar P. 2019. Hypoxic non-replicating persistent *Mycobacterium*
936 *tuberculosis* develops thickened outer layer that helps in restricting rifampicin entry.
937 Front Microbiol 10:2339.
938 **61.** Banerjee S, Nandyala AK, Raviprasad P, Ahmed N, Hasnain SE. 2007. Iron-
939 dependent RNA-binding activity of *Mycobacterium tuberculosis* aconitase. J Bacteriol
940 189:4046-4052.
941 **62.** Rahi A, Dhiman A, Singh D, Lynn AM, Rehan M, Bhatnagar R. 2018. Exploring the
942 interaction between *Mycobacterium tuberculosis* enolase and human plasminogen
943 using computational methods and experimental techniques. J Cell Biochem
944 119:2408-2417.
945 **63.** de la Paz Santangelo M, Gest PM, Guerin ME, Coinçon M, Pham H, Ryan G, Puckett
946 SE, Spencer JS, Gonzalez-Juarrero M, Daher R, Lenaerts AJ, Schnappinger D,

947 Therisod M, Ehrt S, Sygusch J, Jackson M. 2011. Glycolytic and non-glycolytic
948 functions of *Mycobacterium tuberculosis* fructose-1,6-bisphosphate aldolase, an
949 essential enzyme produced by replicating and non-replicating bacilli. J Biol Chem
950 286:40219-40231.
951 **64.** Gengenbacher M, Rao SPS, Pethe K, Dick T. 2010. Nutrient-starved, non-replicating
952 *Mycobacterium tuberculosis* requires respiration, ATP synthase and isocitrate lyase
953 for maintenance of ATP homeostasis and viability. Microbiology 156:81-87.
954 **65.** Nandakumar M, Nathan C, Rhee K. 2014. Isocitrate lyase mediates broad antibiotic
955 tolerance in *Mycobacterium tuberculosis*. Nat Commun 5:4306.
956 **66.** Bhusal RP, Jiao W, Kwai BXC, Reynisson J, Collins AJ, Sperry J, Bashiri G, Leung
957 IKH. 2019. Acetyl-CoA-mediated activation of *Mycobacterium tuberculosis* isocitrate
958 lyase 2. Nat Commun 10:4639.
959 **67.** Daniel J, Maamar H, Deb C, Sirakova TD, Kolattukudy PE. 2011. *Mycobacterium*
960 *tuberculosis* uses host triacylglycerol to accumulate lipid droplets and acquires a
961 dormancy-like phenotype in lipid-loaded macrophages. PLoS Pathog 7:e1002093.
962 **68.** Maurya RK, Bharti S, Krishnan MY. 2018. Triacylglycerols: Fuelling the hibernating
963 *Mycobacterium tuberculosis*. Front Cell Infect Microbiol 8:450.
964 **69.** Pohane AA, Carr CR, Garhyan J, Swarts BM, Siegrist MS. 2021. Trehalose recycling
965 promotes energy-efficient biosynthesis of the Mycobacterial cell envelope. mBio
966 12:e02801-20.
967 **70.** Langklotz S, Narberhaus F. 2011. The *Escherichia coli* replication inhibitor CspD is
968 subject to growth-regulated degradation by the Lon protease. Mol Microbiol 80:1313-
969 1325.
970 **71.** Uppal S, Shetty DM, Jawali N. 2014. Cyclic AMP receptor protein regulates *cspD*, a
971 bacterial toxin gene, in *Escherichia coli*. J Bacteriol 196:1569-1577.

72. Spanka DT, Konzer A, Edelmann D, Berghoff BA. 2019. High-throughput proteomics identifies proteins with importance to postantibiotic recovery in depolarized persister cells. Front Microbiol 10:378.

73. Torrey HL, Keren I, Via LE, Lee JS, Lewis K. 2016. High persister mutants in *Mycobacterium tuberculosis*. PLoS One 11:e0155127.

74. Beites T, O'Brien K, Tiwari D, Engelhart CA, Walters S, Andrews J, Yang H-J, Sutphen ML, Weiner DM, Dayao EK, Zimmerman M, Prideaux B, Desai PV, Masquelin T, Via LE, Dartois V, Boshoff HI, Barry CE, Ehrt S, Schnappinge D. 2019. Plasticity of the *Mycobacterium tuberculosis* respiratory chain and its impact on tuberculosis drug development. Nat Commun 10:4970.

75. Rao SPS, Alonso S, Rand L, Dick T, Pethe K. 2008. The protonmotive force is required for maintaining ATP homeostasis and viability of hypoxic, nonreplicating *Mycobacterium tuberculosis*. Proc Natl Acad Sci U S A. 105:11945-11950.

76. Cook GM, Hards K, Vilchèze C, Hartman T, Berney M. 2014. Energetics of respiration and oxidative phosphorylation in mycobacteria. Microbiol Spectr 2:10.1128/microbiolspec.MGM2-0015-2013.

77. Ganguli G, Mukherjee U, Sonawane A. 2019. Peroxisomes and oxidative stress: Their implications in the modulation of cellular immunity during Mycobacterial infection. Front Microbiol 10:1121

78. Khare G, Nangpal P, Tyagi AK. 2017. 1. Differential roles of iron storage proteins in maintaining the iron homeostasis in *Mycobacterium tuberculosis*. PLoS One 12(1): e0169545.

79. Savijoki K, Nyman TA, Kainulainen V, Miettinen I, Siljamäki P, Fallarero A, Sandholm J, Satokari R, Varmanen P. 2019. Growth mode and carbon source impact the surfaceome dynamics of *Lactobacillus rhamnosus* GG. Front Microbiol 10:1272.

997 **80.** Savijoki K, Miettinen I, Nyman TA, Kortesoja M, Hanski L, Varmanen P, Fallarero A.
998 2020. Growth mode and physiological state of cells prior to biofilm formation affect
999 immune evasion and persistence of *Staphylococcus aureus*. Microorganisms 8:106.
1000 **81.** Cox J, Mann M. 2008. MaxQuant enables high peptide identification rates,
1001 individualized p.p.b.-range mass accuracies and proteome-wide protein
1002 quantification. Nat Biotechnol 26:1367-1372.
1003 **82.** Cox J, Neuhauser N, Michalski A, Scheltema RA, Olsen JV, Mann M. 2011.
1004 Andromeda: a peptide search engine integrated into the MaxQuant environment. J
1005 Proteome Res 10:1794-1805.
1006 **83.** Deutsch EW, Csordas A, Sun Z, Jarnuczak A, Perez-Riverol Y, Ternent T, Campbell
1007 DS, Bernal-Llinares M, Okuda S, Kawano S, Moritz RL, Carver JJ, Wang M,
1008 Ishihama Y, Bandeira N, Hermjakob H, Vizcaino JA. 2017. The ProteomeXchange
1009 consortium in 2017: supporting the cultural change in proteomics public data
1010 deposition. Nucleic Acids Res 45:D1100-D1106.
1011 **84.** Altschul SF, Gish W, Miller W, Myers EW, Lipman DJ. 1990. Basic local alignment
1012 search tool. J Mol Biol 215:403-410.
1013 **85.** Altschul SF, Madden TL, Schaffer AA, Zhang J, Zhang Z, Miller W, Lipman DJ. 1997.
1014 Gapped BLAST and PSI-BLAST: a new generation of protein database search
1015 programs. Nucleic Acids Res 25:3389-3402.
1016 **86.** Altschul SF, Wootton JC, Gertz EM, Agarwala R, Morgulis A, Schaffer AA, Yu YK.
1017 2005. Protein database searches using compositionally adjusted substitution
1018 matrices. FEBS J 272:5101-5109.
1019 **87.** Marchler-Bauer A, Bo Y, Han L, He J, Lanczycki CJ, Lu S, Chitsaz F, Derbyshire MK,
1020 Geer RC, Gonzales NR, Gwadz M, Hurwitz DI, Lu F, Marchler GH, Song JS, Thanki
1021 N, Wang Z, Yamashita RA, Zhang D, Zheng C, Geer LY, Bryant SH. 2017.

CDD/SPARCLE: functional classification of proteins via subfamily domain architectures. Nucleic Acids Res 45:D200-D203.

88. Ashburner M, Ball CA, Blake JA, Botstein D, Butler H, Cherry JM, Davis AP, Dolinski K, Dwight SS, Eppig JT, Harris MA, Hill DP, Issel-Tarver L, Kasarskis A, Lewis S, Matese JC, Richardson JE, Ringwald M, Rubin GM, Sherlock G. 2000. Gene ontology: tool for the unification of biology. The Gene Ontology Consortium. Nat Genet 25:25-29. doi:10.1038/75556.

89. Rice P, Longden I, Bleasby A. 2000. EMBOSS: the European Molecular Biology Open Software Suite. Trends Genet 16:276-277. doi:10.1016/s0168-9525(00)02024-2.

90. Petersen TN, Brunak S, von Heijne G, Nielsen H. 2011. SignalP 4.0: discriminating signal peptides from transmembrane regions. Nat Methods 8:785-786. doi:10.1038/nmeth.1701.

91. Bendtsen JD, Kiemer L, Fausboll A, Brunak S. 2005. Non-classical protein secretion in bacteria. BMC Microbiol 5:58. doi:10.1186/1471-2180-5-58.

92. Krogh A, Larsson B, von Heijne G, Sonnhammer EL. 2001. Predicting transmembrane protein topology with a hidden Markov model: application to complete genomes. J Mol Biol 305:567-80. doi:10.1006/jmbi.2000.4315.

93. Sonnhammer EL, von Heijne G, Krogh A. 1998. A hidden Markov model for predicting transmembrane helices in protein sequences. Proc Int Conf Intell Syst Mol Biol 6:175-182. doi:10.1006/jmbi.2000.4315.

94. Tyanova S, Temu T, Sinitcyn P, Carlson A, Hein MY, Geiger T, Mann M, Cox J. 2016. The Perseus computational platform for comprehensive analysis of (prote)omics data. Nat Methods 13:731-740.

1046 **95.** Szklarczyk D, Gable AL, Lyon D, Junge A, Wyder S, Huerta-Cepas J, Simonovic M,
1047 Doncheva NT, Morris JH, Bork P, Jensen LJ, von Mering C. 2019. STRING v11:
1048 protein-protein association networks with increased coverage, supporting functional
1049 discovery in genome-wide experimental datasets. Nucleic Acids Res 47:D607-613

1050

1051 **LEGENDS for figures and tables**

1052 **Figure 1.** Mmr biofilms show distinct growth morphologies after two-weeks of growth.
1053 SBFs grow with lichen-like structures, whereas PBFs have a ribbon-like cords morphology,
1054 which becomes more defined with maturation (after 3 weeks). The WDeM images are
1055 maximum- intensity projections of one-, two-, and three-week-old biofilms (a) together with
1056 an image where Z-position is color-coded (b). X/Y scale bar corresponds to 10 µm and
1057 frame interval is 2µm.

1058 **Figure 2. (A)** A workflow depicting the conditions and time points used for preparing the
1059 planktonic and biofilm cells of Mmr. Grey arrows indicate sampling time points for pellicle
1060 (PBF) and submerged (SBF) biofilms. (B) Workflow used for identification of surface
1061 proteins associated with planktonic (PL_log) cells, PBFs and SBFs. Marker proteins were
1062 identified by comparing the raw intensity data, statistically significant protein abundance
1063 changes by pairwise comparisons of the log2 converted LFQ data and the protein co-
1064 abundance patterns by subjecting the LFQ data to imputation and z-score normalization.
1065 STRING and pathway enrichment analyses were conducted on the selected heat-map
1066 clusters and necessary phenotypic assays to validate the key proteome differences.

1067 **Figure 3.** The most significant protein abundance fold changes between the indicated cell
1068 types at selected timepoints. The log2 transformed LFQ data was analyzed
1069 using Student's t-test with permutation-based FDR adjustment. In the first two top panels,
1070 the fold-change x 1000.

Figure 4. (A) Comparison of relative transcript abundance for *celA1* between the Mmr-CelA1 overexpression strain and the Mmr control strain with pTEC27 (WT). The CelA1 overexpression levels were normalized to the expression level of CelA1 in the WT control. The data is obtained from two technical replicates from two different bacterial clones. The bars represent the standard deviation. CelA1 expression is normalized with the amount of Mmar DNA in each sample. **(B)** CelA1 overexpression disrupts the biofilm development, and the formation of the subtype-specific growth morphologies. The WDeM images are maximum intensity projections of the two-week-old Mmr control biofilms (pTEC27, WT) and the Mmr-CelA1 cultures (a), together with color-coded by Z-position images (b). Scale bars 100 µm and frame interval is 2µm. **(C)** The MIC/MBC of rifampicin is reduced in both the PL and biofilms formed with the CelA1 overexpressing strain compared to the Mmr control cultures (PTEC27, WT). Rifampicin was added to the liquid cultures two, four, seven and 14 days after the start of the culture. Ten µl per sample (in triplicate) was plated seven days after the addition of rifampicin and CFUs were counted seven days thereafter. 100 CFU per sample was used as the cut-off limit for bacterial growth. The experiment was carried out three times. The figure shows a representative experiment. **-**, = no growth, + = bacterial growth , UNT= untreated

Figure 5. (A) A PCA analysis of all detected proteins (based on LFQ intensities excluding one SBF_3w outlier) with PC1 and PC2 indicating growth mode- and time point-dependent changes. **(B)** Hierarchical clustering of proteins (complete linkage; n, 690) with significantly changed expression profiles. Color intensity: red and green indicate higher and lower protein abundances, respectively.

Figure 6. (A) A PPI network analysis on cluster 1 proteins (Fig. 5B) with higher abundancies on SBFs between two and four weeks. No. nodes, 368; no. edges, 3256; PPI enrichment $P < 1.0e\text{-}16$. **(B)** A PPI network analysis on cluster six proteins with higher

abundancies on SBFs between two days and 2 weeks. Proteins were clustered using MCL with the inflation parameter set to 4.0 (cluster 6) and 6.0 (cluster 1). No. nodes, 155; no. edges, 3024; PPI enrichment P < 1.0e-16. Circles indicate the most enriched protein interactions.

Figure 7. A schematic model of the Mmr cell envelope with key protein abundance changes specific to PL, PBF and SBF cells. Colored arrows pointing up/down refer to protein abundances/abundance changes within the indicated cell sample types (green, PL; blue, PBFs; red, SBFs). MA, mycolic acids; cMAs, cyclopropanated mycolic acids; TDM/TMM, trehalose-6,6-dimycolate/trehalose monomycolate; PDIM/PGL, phthiocerol dimycoceros- ates/phenolic glycolipids. C, cytoplasm; IM, inner membrane; PP, periplasmic space; AG, arabinogalactan; PG, peptidoglycan; MM, mycomembrane; ECM, extracellular matrix.

Figure 8. The proportion of persistent bacterial cells increases in Mmr biofilms. Time-kill curve analysis was performed by culturing biofilms from two days to two weeks and treating the bacteria with 400 µg mL^{-1} rifampicin. The killing kinetics were monitored for seven days by measuring the bioluminescence signal produced by Lux-Mmr daily. **(A)** Logarithmic growth phase planktonic and 2-week-old biofilm Mmr were treated with 400 µg mL^{-1} of rifampicin. The time-kill curves of the planktonic and biofilm-associated bacteria were significantly different (P < 0.0034, log-rank test). The means and SEMs of three biological replicates are shown. **(B)** In biofilms, persistence increases over time and is significantly higher after one week compared to planktonic bacteria (P = 0.0002, log-rank test). Planktonic culture and two-day-old biofilm show similar killing curves. Means and SEMs of three biological replicates are shown. **(C)** Two-week-old PBFs and SBFs were tested separately for persistence. The two different biofilm-types show no difference in

their persistence levels (*P* = 0.51, log-rank test). Means and SEMs of three biological replicates are shown.

SUPPLEMENTAL MATERIAL

Figure S1. (A) Pellicle-type (PBF) and submerged (SBF) biofilms after culturing for two weeks (left) and 12 weeks (right). **(B)** Distribution of overlapping protein identifications within four replica samples from planktonic cell surfaces and biofilm-ECMs. PL_log, logarithmic planktonic cells; SBF, submerged type biofilms; PBF, pellicle type biofilms.

Figure S2. (A) Distribution of identified proteins in terms of their predicted secretion motifs and the number of predicted TMDs. PL_log, logarithmic planktonic cells; PBF_all and SBF_all, all identified proteins from pellicle and submerged biofilm matrices, respectively. Other, proteins without any known motifs for classical or non-classical secretion. **(B)** Venn diagrams indicating the core and marker proteomes within all identifications (planktonic and biofilms) at each time point.

Figure S3. (A) The bioluminescence-based readout of the biofilm killing assay was validated using the OD_{600}–method to monitor bacterial growth at varying time points of growth, showing similar killing kinetics as observed with the bioluminescence measurements of the same samples. Here, the four-day-old biofilm and two-day-old planktonic cells were treated with 200 µg mL^{-1} rifampicin. The mean of three biological replicates of the OD_{600}-based assay is shown. **(B)** Mmr growth is accompanied by increased bioluminescence values in maturing biofilms without the antibiotic treatment, even at timepoints of over one week of biofilm culture. The bioluminescence was measured three times/three seconds using EnVision equipment (Perkin Elmer), and the mean of relative light units (RLUs) per one second was calculated. Means and SEMs of three biological replicates are shown.

Table S1. List of all proteins identified on Mmr cells during different growth modes. The colored cells refer to the average (log2) raw intensity values for proteins detected in at least two replica samples. Cells in grey, protein was not detected. PL_log, logarithmic planktonic cells; PBF, pellicle type biofilm cells; SBF, submerged type biofilm cells.

Table S2. Proteins specific to pellicle biofilms (PBFs), submerged biofilms (SBFs) and to both biofilms that lack an identifiable counterpart on planktonic cell surfaces. Proteins detected in each replica samples are shown. Color gradient bar refers to log2-transformed raw intensity values (avr., n ≥ 2): blue, low abundance; yellow, high abundance; PBF, pellicle biofilm; SBF, submerged biofilm.

Table S3. Log2-transformed MaxLFQ data with minimum of two valid identifications (out of four) in at least one group, and statistically significant protein abundance changes between the PL and PBF_2, PL and SBF-2d, PBF_2w_SBF_2d, PBF_12w and SBF_12w, PBF_4w and 12w and SBF_4w and 12w.

Table S4. Statistically significant protein abundance changes within planktonic cell surfaces and biofilm-ECMs. Colored cells in column "Cluster" correspond to those used in the heat-map (Fig. 5). Significant changes were calculated using a multiple-sample test (ANOVA model, FDR < 0.05, S0 = 0.1). Color intensity code bar below, blue - low abundance; yellow - high abundance.

Table S5. Functional enrichment analysis (GO, KEGG, InterPro, Pham) on cluster 1, 2 and 6 proteins (Figure 5) were studied using the STRING database v. 11 with both the rank- and gene set-based approaches (FDR of 0.05).

Table S6. Key proteome changes within the planktonic cell surfaces and biofilm matrices at different time points of growth. Gradient bar, normalized identification intensity values (avg. ≥ 3).

Table S7. Colony ability of non-shaved and enzymatically shaved biofilm and planktonic cells. Biofilm cells were cultured for two weeks and planktonic cells for two days, as described in material and methods. Cells in three biological replicates were suspended in trypsin/Lys-C digestion buffer and then divided into two aliquots; the first aliquot was taken as the non-shaved cell control containing only the digestion buffer, and the second aliquot of cells was treated with the trypsin/Lys-C enzyme. After 20 min incubation at 37 °C, the cell suspensions were suspended gently in PBS containing 0.2% Tween80 (v/v) and serially diluted cells were spotted in four technical replicates (10 uL each) on an agar plate. After one week cultivation at 37 °C, the colonies were calculated and compared under different conditions. nd, colonies could not be counted due to the presence of cell aggregates.

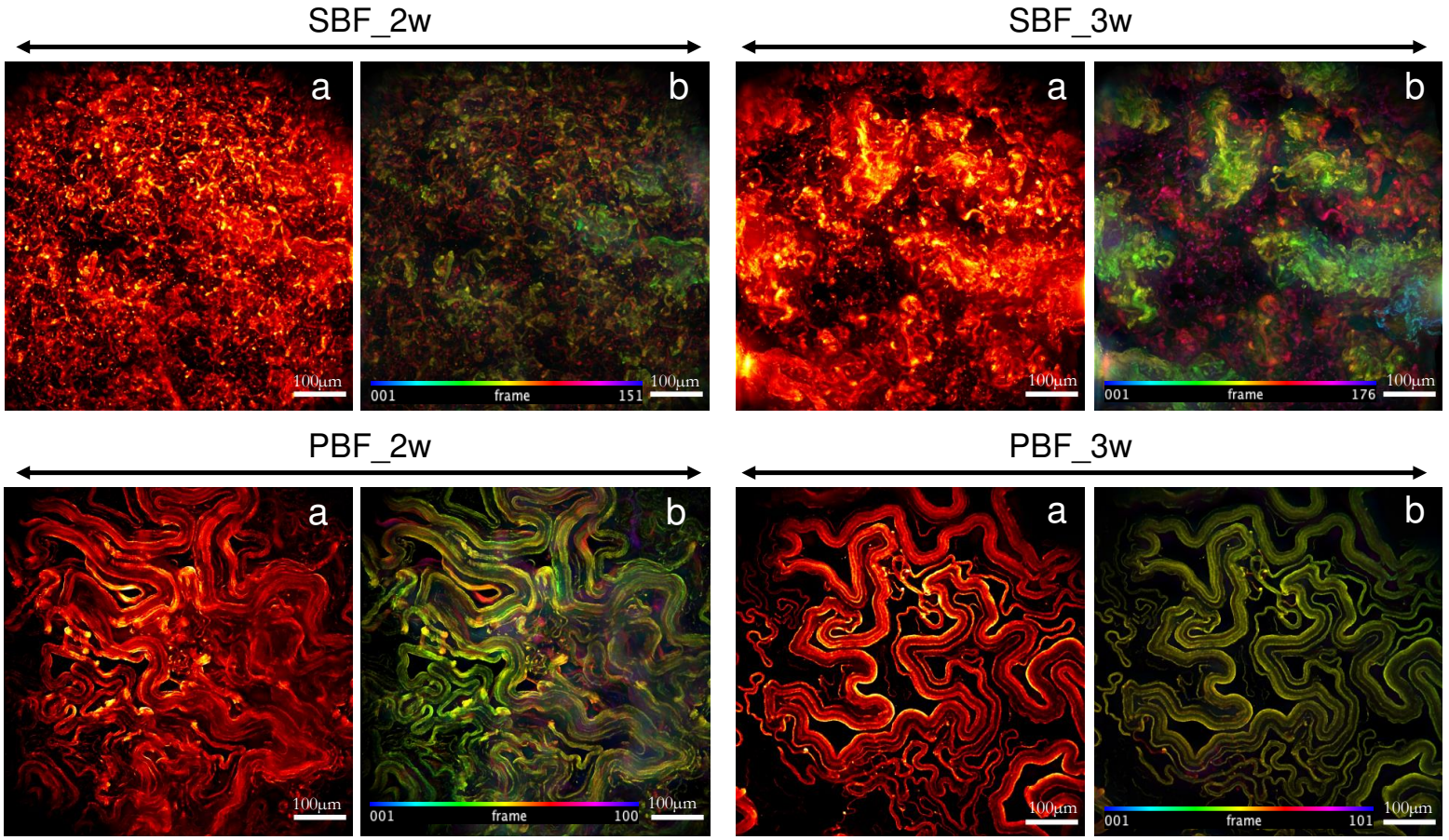

Fig. 1

Fig. 2

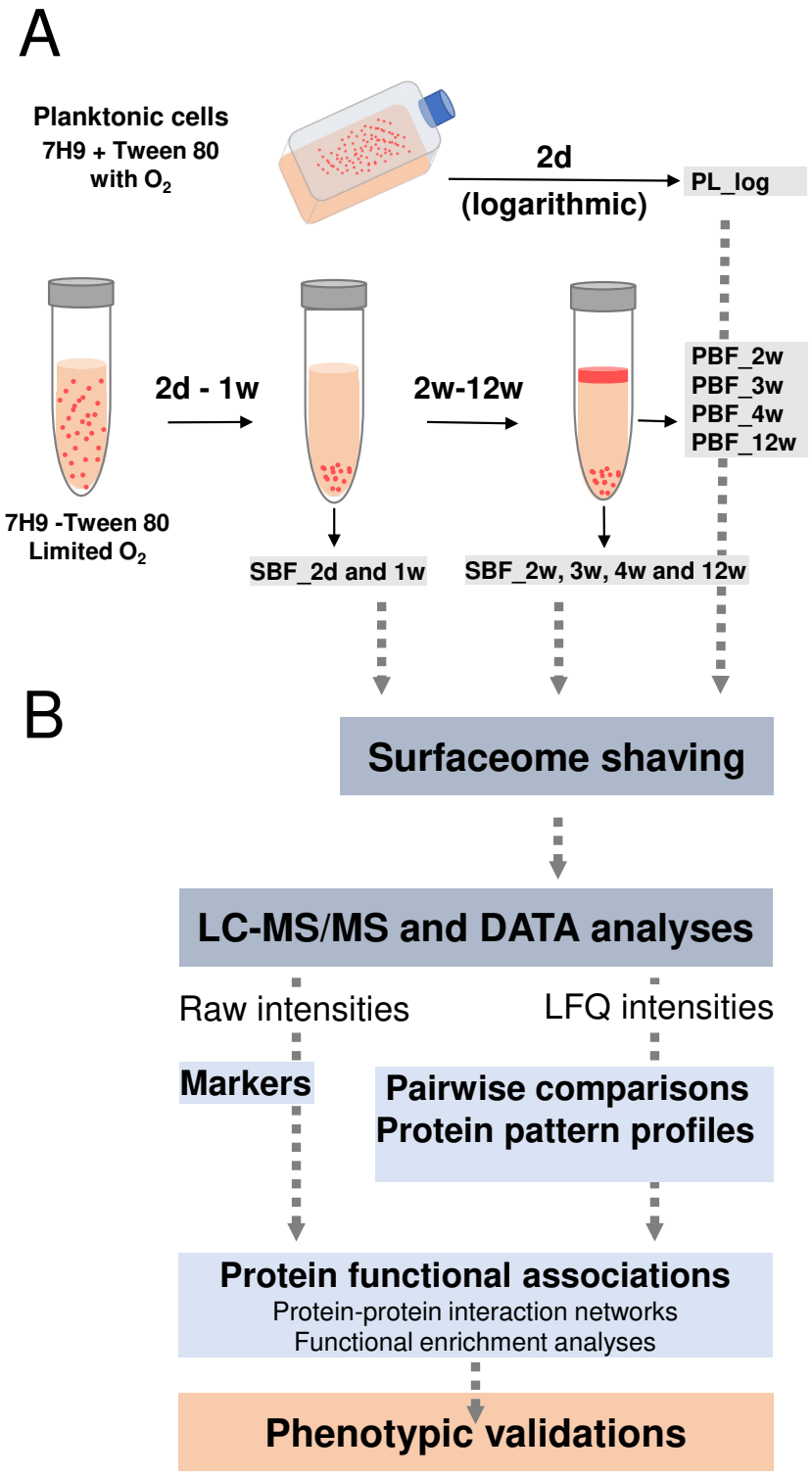
A
Planktonic cells
7H9 + Tween 80
with O_2
2d
(logarithmic)
PL_log
2d - 1w
2w-12w
PBF_2w
PBF_3w
PBF_4w
PBF_12w
7H9 -Tween 80
Limited O_2
SBF_2d and 1w
SBF_2w, 3w, 4w and 12w
B
Surfaceome shaving
LC-MS/MS and DATA analyses
Raw intensities
LFQ intensities
Markers
Pairwise comparisons
Protein pattern profiles
Protein functional associations
Protein-protein interaction networks
Functional enrichment analyses
Phenotypic validations

Fig. 3

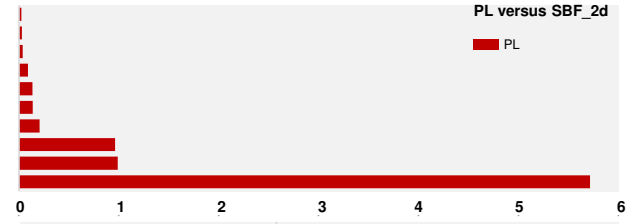

Immunogenic protein MPB64
Antigen 85C
Hypothetical lipoprotein LpqF
Cutinase - Cut
Cellulose hydrolase - CelA1
MHB domain-containing protein
PPE family protein
PPE family protein
CwlM
PPE family protein, PPE61

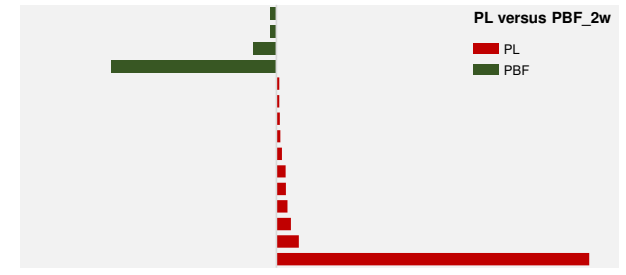

ESAT-6-like protein
APA - alanine and proline rich protein
ESX-1 secretion protein EspF
EspA/EspE protein
PPE family protein
Cutinase - Cut
Uncharacterized protein
Low molecular weight antigen
Isocitrate lyase ICL1
PPE family protein
Cellulose hydrolase - CelA1
Peptidoglycan synthesis associated ligase - MurE
PPE family protein
Peptidoglycan hydrolase - CwlM
PPE family protein, PPE61

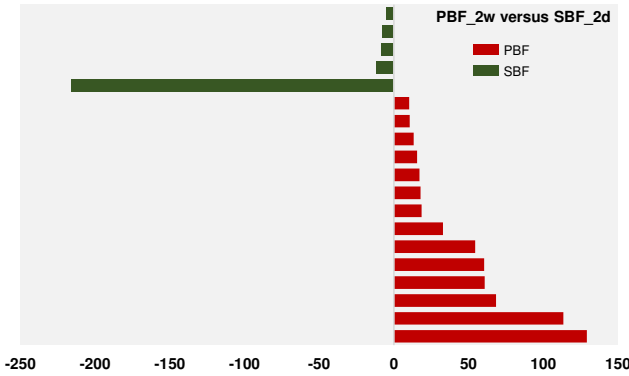

Long-chain-fatty-acid-AMP ligase FadD29
ATP-dependent RNA helicase RhlE
Uroporphyrin-III C-methyltransferase HemD
Haloacid dehalogenase
Isocitrate lyase- ICL1
ESX-1 secretion-associated protein EspB
Lipoprotein
MPT51/MPB51 antigen
ESAT-6-like protein
Acid phosphatase
APA - alanine and proline rich protein
Peptidoglycan endopeptidase RipA
Cutinase
ESAT-6-like protein
PPE family protein
EspA/EspE protein
DUF4185 domain-containing protein
PPE family protein
ESX-1 secretion-associated protein EspF

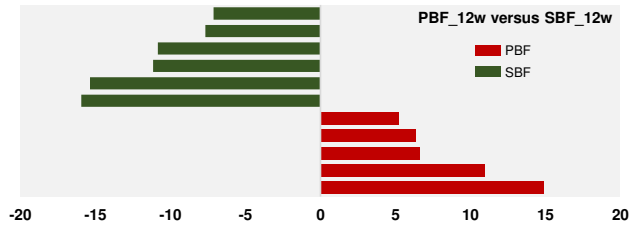

Isocitrate lyase - ICL1
Beta-lactamase
Long-chain-fatty-acid-AMP ligase FadD29
Biotin synthase
Uroporphyrin-III C-methyltransferase HemD
A0A117DW50_9MYCO Putative secreted protein
Limonene 1,2-monooxygenase
Transcriptional regulator MraZ
Elongation factor G FusA2
Protein translocase subunit SecE
N-acetylmuramic acid (MurNAc) residue deacetylace PdaC

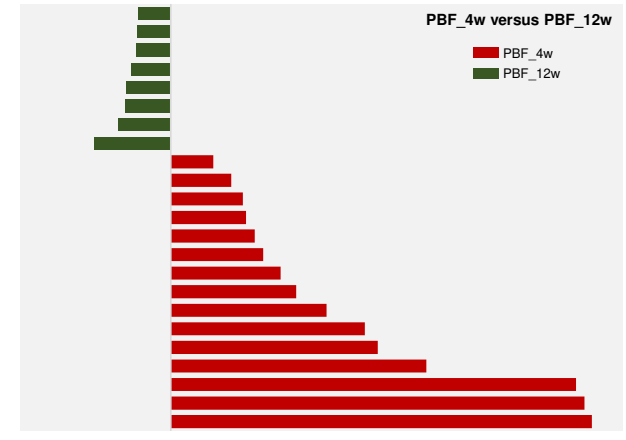

Pyruvate-flavodoxin oxidoreductase
Cytochrome D ubiquinol oxidase (Subunit I) CydA
Aldehyde-alcohol dehydrogenase
Acyl-ACP desaturase
AMP-dependent synthetase
Pyruvate dehydrogenase component
Histidine kinase
SRPBCC ligand-binding domain superfamily protein
APA - alanine and proline rich protein
HHDD isomerase + cyclase/dehydrase
Serine protease PepA
Cutinase
Fibronectin attachment protein FAP
A0A2Z5YMU1_MYCMR Protease
Acid phosphatase
Peptidyl-prolyl cis-trans isomerase
ESAT-6-like protein
A membrane protein, MmpS5_2
A0A100I977_9MYCO Secreted protein
ESX-1 secretion-associated protein EspF
ESAT-6-like protein
EspA/EspE protein
Immunogenic protein MPB64

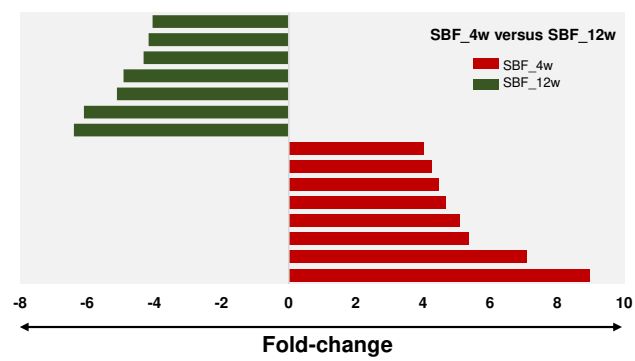

α-1,4-glucan:maltose-1-phosphate maltosyltransferase
Histidine kinase
MCE-family protein Mce1A
MCE-family protein Mce1B
PmbA_TldD peptidase
Mammalian cell entry protein MCE
GTP cyclohydrolase 1
Protein-export membrane protein SecF
Acid resistance periplasmic serine protease MarP
Protein translocase subunit SecE
Arabinosyltransferase EmbB
Type VII serine protease MycP
EspA/EspE protein
Arabinosyltransferase EmbA
Large-conductance mechanosensitive channel MscL protein

Fig. 4

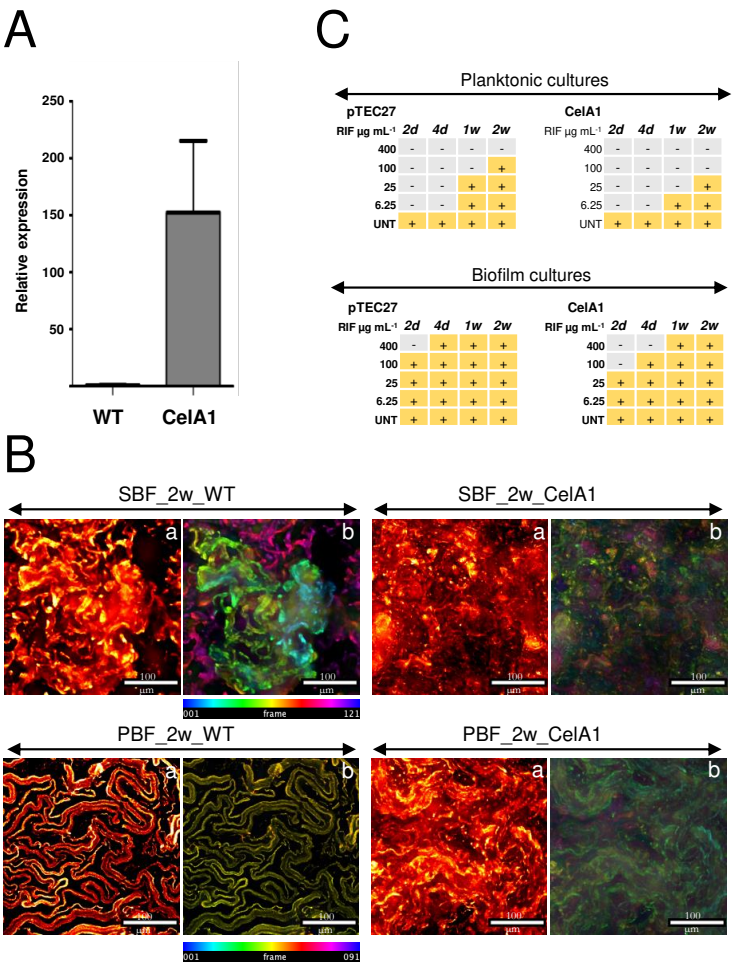
A
Relative expression
250
200
150
100
50
WT
CelA1
C
Planktonic cultures
pTEC27
RIF µg mL-1 2d 4d 1w 2w
400 - - - -
100 - - - +
25 - - + +
6.25 - - + +
UNT + + + +
CelA1
RIF µg mL-1 2d 4d 1w 2w
400 - - - -
100 - - - -
25 - - - +
6.25 - - + +
UNT + + + +
Biofilm cultures
pTEC27
RIF µg mL-1 2d 4d 1w 2w
400 - + + +
100 + + + +
25 + + + +
6.25 + + + +
UNT + + + +
CelA1
RIF µg mL-1 2d 4d 1w 2w
400 - - + +
100 - + + +
25 + + + +
6.25 + + + +
UNT + + + +
B
SBF_2w_WT
SBF_2w_CelA1
PBF_2w_WT
PBF_2w_CelA1
a
b
100 µm
001 frame 121
001 frame 091

A

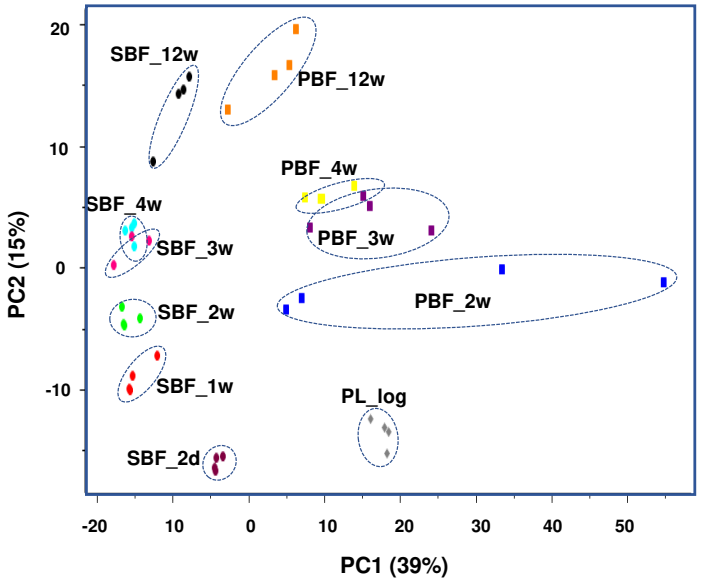
SBF_12w
PBF_12w
PBF_4w
SBF_4w
SBF_3w
PBF_3w
PBF_2w
SBF_2w
SBF_1w
PL_log
SBF_2d
PC2 (15%)
PC1 (39%)
20
10
0
-10
-20
10
0
10
20
30
40
50

B

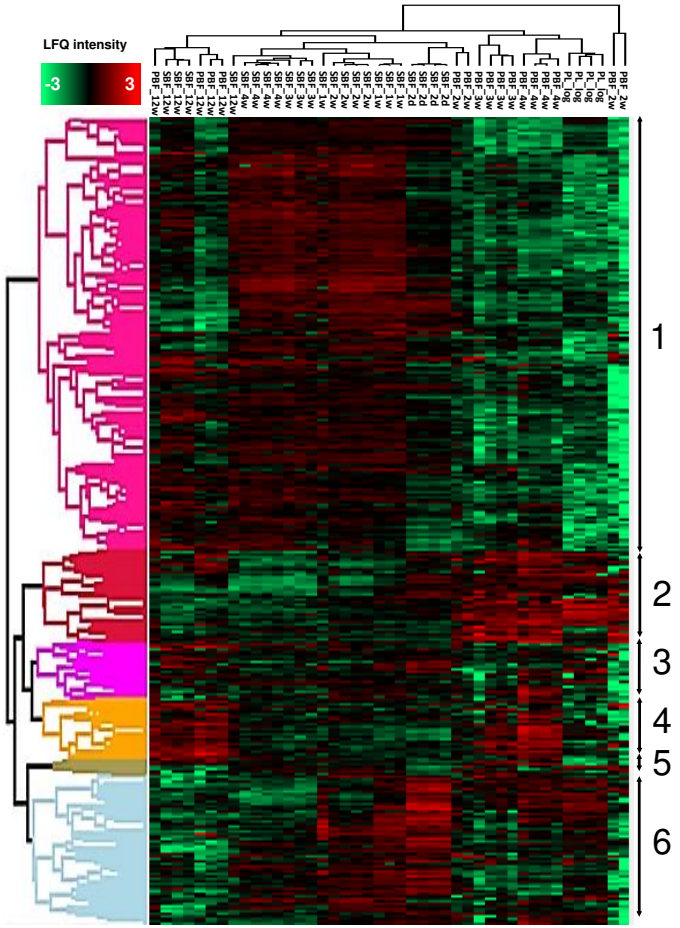
LFQ intensity
-3
3
1
2
3
4
5
6

Fig. 5

A

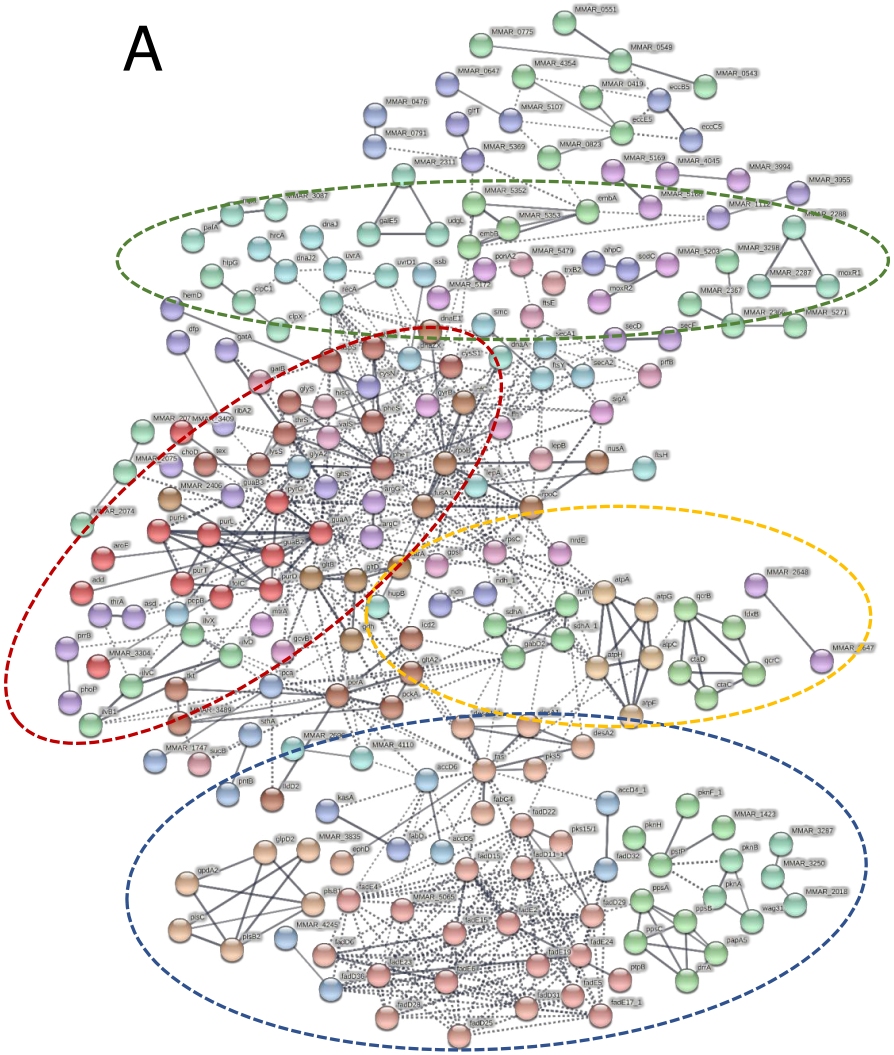

B

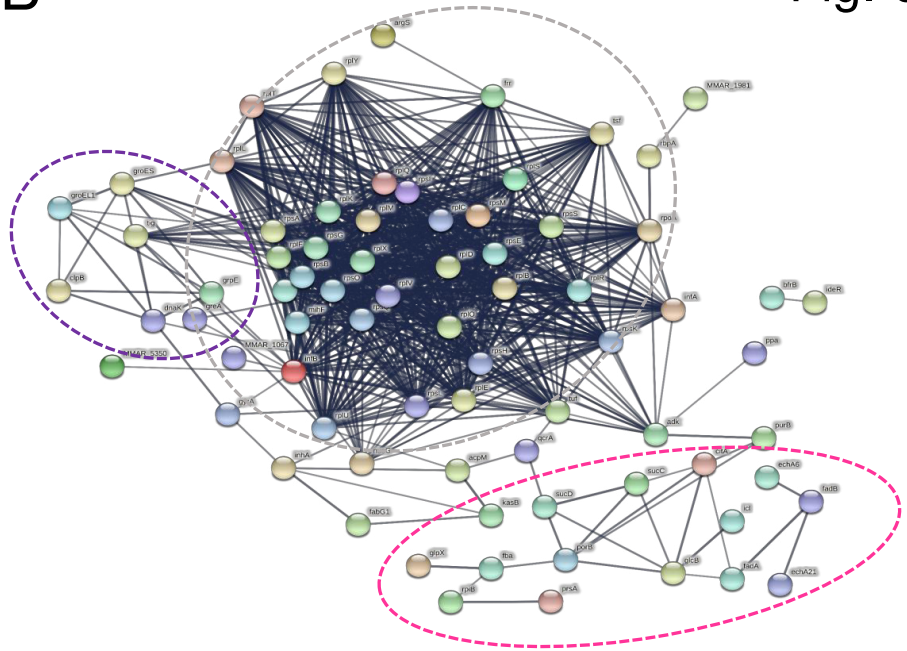

Fig. 6

- Amino acid biosynthesis
- Stress response
- Respiratory electron transfer and ATP synthesis
- Fatty acid biosynthesis and aerobic β-oxidative degradation fatty acids
- Translation (r-proteins)
- Glycolysis and TCA cycle

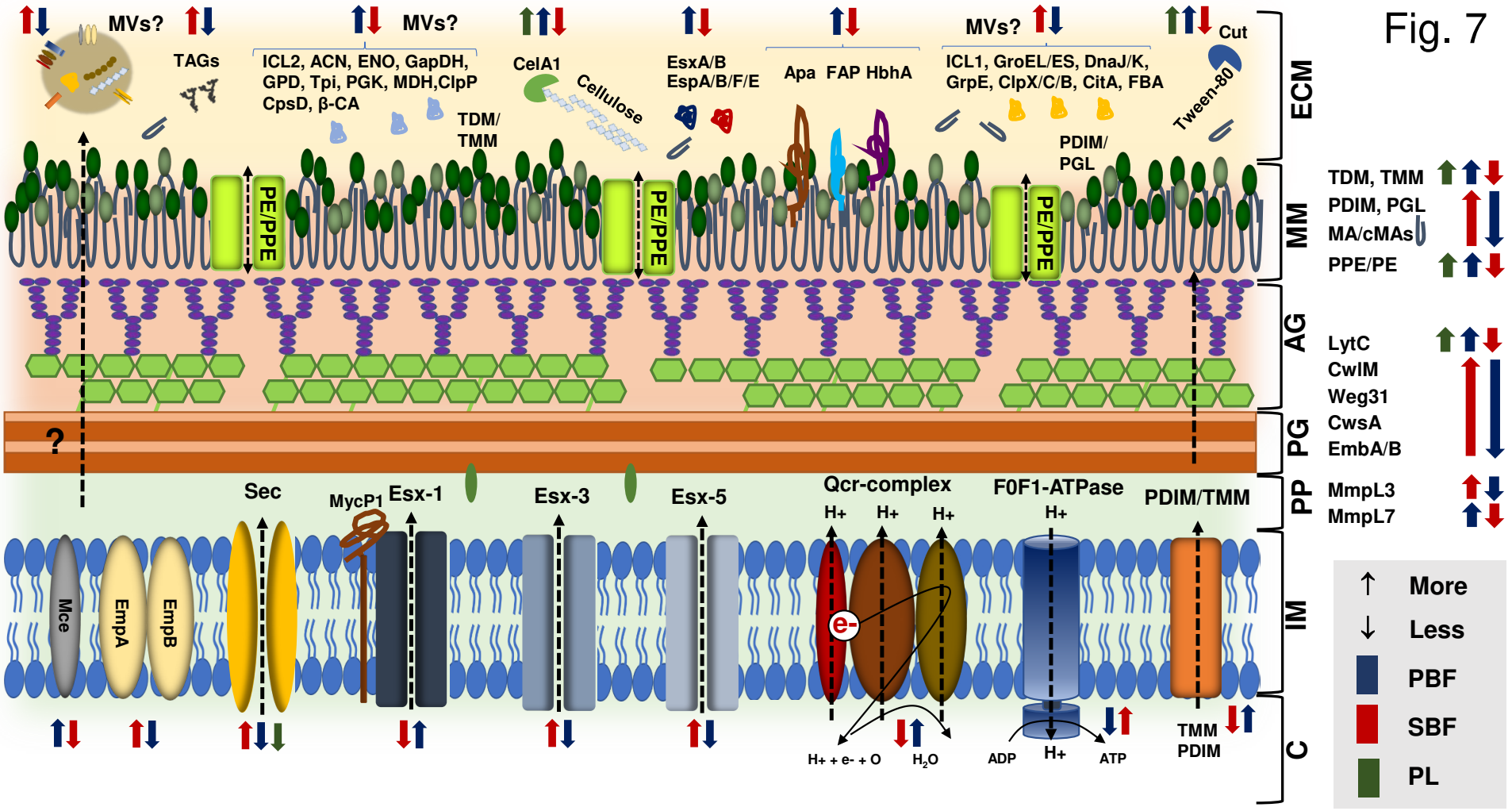
MVs?
TAGs
MVs?
ICL2, ACN, ENO, GapDH, GPD, Tpi, PGK, MDH,ClpP CpsD, β-CA
TDM/ TMM
CelA1
Cellulose
EsxA/B EspA/B/F/E
Apa FAP HbhA
MVs?
ICL1, GroEL/ES, DnaJ/K, GrpE, ClpX/C/B, CitA, FBA
PDIM/ PGL
Cut
Tween-80
PE/PPE
PE/PPE
PE/PPE
ECM
MM
AG
PG
PP
IM
C
?
Sec
MycP1
Esx-1
Esx-3
Esx-5
Qcr-complex
F0F1-ATPase
PDIM/TMM
Mce
EmpA
EmpB
H+
e-
H+ + e- + O
H2O
ADP
ATP
TMM
PDIM
TDM, TMM
PDIM, PGL
MA/cMAs
PPE/PE
LytC
CwlM
Weg31
CwsA
EmbA/B
MmpL3
MmpL7
More
Less
PBF
SBF
PL

Fig. 7

Fig. 8

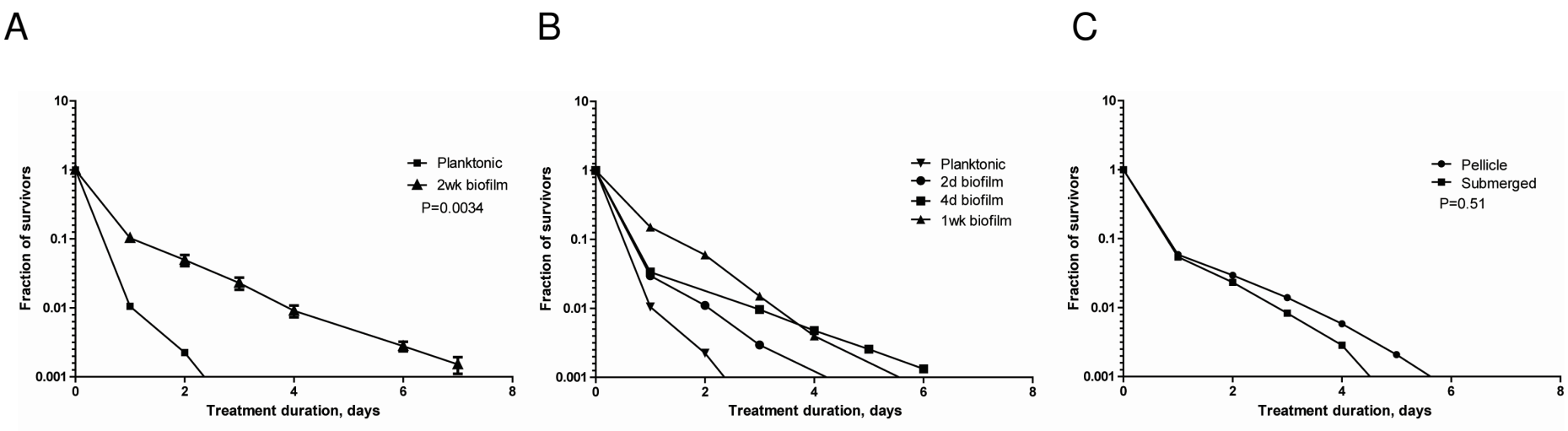
A
B
C
Fraction of survivors
Treatment duration, days
Planktonic
2wk biofilm
P=0.0034
Planktonic
2d biofilm
4d biofilm
1wk biofilm
Pellicle
Submerged
P=0.51